


Singlet oxygen-induced signalling depends on the metabolic status of the *Chlamydomonas reinhardtii* cell

Waeil Al Youssef ¹, Regina Feil², Maureen Saint-Sorny ³, Xenie Johnson ³, John E. Lunn ², Bernhard Grimm ¹ & Pawel Brzezowski ¹ 

Using a mutant screen, we identified trehalose 6-phosphate phosphatase 1 (TSPP1) as a functional enzyme dephosphorylating trehalose 6-phosphate (Tre6P) to trehalose in *Chlamydomonas reinhardtii*. The *tspp1* knock-out results in reprogramming of the cell metabolism via altered transcriptome. As a secondary effect, *tspp1* also shows impairment in ¹O₂-induced chloroplast retrograde signalling. From transcriptomic analysis and metabolite profiling, we conclude that accumulation or deficiency of certain metabolites directly affect ¹O₂-signalling. ¹O₂-inducible *GLUTATHIONE PEROXIDASE 5 (GPX5)* gene expression is suppressed by increased content of fumarate and 2-oxoglutarate, intermediates in the tricarboxylic acid cycle (TCA cycle) in mitochondria and dicarboxylate metabolism in the cytosol, but also myo-inositol, involved in inositol phosphate metabolism and phosphatidylinositol signalling system. Application of another TCA cycle intermediate, aconitate, recovers ¹O₂-signalling and *GPX5* expression in otherwise aconitate-deficient *tspp1*. Genes encoding known essential components of chloroplast-to-nucleus ¹O₂-signalling, PSBP2, MBS, and SAK1, show decreased transcript levels in *tspp1*, which also can be rescued by exogenous application of aconitate. We demonstrate that chloroplast retrograde signalling involving ¹O₂ depends on mitochondrial and cytosolic processes and that the metabolic status of the cell determines the response to ¹O₂.

¹ Pflanzenphysiologie, Institut für Biologie, Humboldt-Universität zu Berlin, 10115 Berlin, Germany. ² Max Planck Institute of Molecular Plant Physiology, 14476 Potsdam-Golm, Germany. ³ Photosynthesis and Environment Team, Commissariat à l'Énergie Atomique et aux Énergies Alternatives (CEA), CNRS, Institut de Biosciences et Biotechnologies d'Aix-Marseille, Aix-Marseille Université, UMR 7265, CEA Cadarache, F-13108 Saint-Paul-lez-Durance, France. email: pawel.brzezowski@hu-berlin.de

Nearly 40 years ago, tetrapyrrole biosynthesis (TBS) intermediates were proposed to be involved in chloroplast retrograde (organelle-to-nucleus) signalling. This conclusion was based on the observation that accumulation of chlorophyll precursors negatively affects transcript level of light-harvesting chlorophyll a/b-binding (LHCB) protein¹. Later studies on chloroplast retrograde signalling involved mutants², treatment with a carotenoid biosynthesis inhibitor, norflurazon³, or TBS inhibitors, such as α,α -dipyridyl¹ or thujaplicin⁴. Experiments with norflurazon led to the discovery of the *genomes uncoupled* (*gun*) mutants with a common phenotype of chloroplast status-independent expression of photosynthesis-associated nuclear genes³.

It is noteworthy that treatment with inhibitors causing carotenoid deficiencies results in generation of reactive oxygen species (ROS) and photooxidative damage to chloroplasts. Furthermore, the end-products of TBS, heme and chlorophyll, as well as many of their intermediates (Supplementary Fig. 1) are light-absorbing and redox-reactive molecules, capable to generate ROS. Singlet oxygen ($^1\text{O}_2$) can be produced through interaction of ground (triplet)-state oxygen ($^3\text{O}_2$) with triplet-state chlorophyll or TBS intermediates, e.g. protoporphyrin IX (Proto), which are excited by light⁵. ROS are also metabolic products of other cellular processes in plants, such as photosynthesis and respiration.

Although $^1\text{O}_2$ is not considered to be the most reactive oxygen species, it is thought to be the major ROS involved in photooxidative damage⁶. However, it was shown that production of $^1\text{O}_2$ in the chloroplast induces stress responses that do not result exclusively from physicochemical damage, but also rely on signal transduction triggered by ROS⁷. $^1\text{O}_2$ has a short half-life (about 200 ns) in the cell⁸ and as a result, the distance that it may move was calculated to be ~ 10 nm, based on predicted diffusion rates^{9,10}. Its diffusion range is also limited due to its high reactivity with membrane lipids¹¹. Therefore, $^1\text{O}_2$ could play a specific role as an activator of a stress response only if it is detected close to its source, which strongly suggests that other components mediating the $^1\text{O}_2$ signals should exist. Alternatively, altered metabolite contents triggered by $^1\text{O}_2$ may also mediate $^1\text{O}_2$ -retrograde signalling, or certain metabolic signature may be required to trigger changes in nuclear gene expression^{12,13}.

Despite the profound effect of $^1\text{O}_2$ on the chloroplast redox state and its apparent involvement in altering nuclear gene expression, little is known about the components involved in $^1\text{O}_2$ -dependent retrograde signalling. The protein factors identified so far include executor 1 (EX1) and EX2 in the *fluorescence* (*flu*) mutant of *Arabidopsis thaliana*¹⁴, the P-subunit of photosystem II family protein (PSBP2)¹⁵ and singlet oxygen acclimation knockedout 1 (SAK1) in *Chlamydomonas reinhardtii*¹⁶, or methylene blue sensitivity (MBS1) shown to be involved in $^1\text{O}_2$ -signalling in both *A. thaliana* and *C. reinhardtii*¹⁷.

We hypothesized that $^1\text{O}_2$ generated via the photosensitizing activity of Proto triggers signalling cascades that alter nuclear gene expression. Therefore, we used a *C. reinhardtii* mutant *chLD-1*¹⁸ that does not produce chlorophyll and accumulates Proto due to a dysfunctional Mg-chelatase (MgCh, Supplementary Fig. 1), but with introduced over-expression of the gene encoding the *genomes uncoupled 4* (GUN4) protein, *chLD-1/GUN4*¹⁹. Endogenous accumulation of Proto in mutants is advantageous for studying $^1\text{O}_2$ -signalling, because it eliminates the need for exogenous application of TBS or carotenoid biosynthesis inhibitors, as well as photosensitizers, such as rose bengal or neutral red to induce $^1\text{O}_2$ generation^{15,20,21}, which are not natural products of the cell, do not localise specifically to any subcellular compartment, and as a consequence may result in artefactual responses. In these terms, the system used in our study is similar to the research conducted on the conditional *flu* mutant of *A. thaliana*.

However, instead of Proto, etiolated seedlings of *flu* accumulate another TBS intermediate, protochlorophyllide (Pchlde; Supplementary Fig. 1), which generates $^1\text{O}_2$ in light²². Nonetheless, it should be noted that neither accumulation of Pchlde in *A. thaliana* nor accumulation of Proto in *C. reinhardtii* can be observed in their respective wild types (WTs) in any conditions, and both systems were artificially generated to facilitate study of the $^1\text{O}_2$ -signalling. In contrast to *flu*, which shows WT level of chlorophyll in continuous light²³, *C. reinhardtii* mutant used in our study is devoid of chlorophyll and accumulates Proto both in dark and light. The lack of chlorophyll in the mutants used in our study provides another advantage, because such mutants do not have functional photosynthetic electron transport (PET), so that $^1\text{O}_2$ production and signalling originating in photosynthesis is avoided. The accumulating Proto is thus the dominant source of generated $^1\text{O}_2$ in the chloroplast and we hypothesized that this approach should allow us to isolate novel components or mechanisms governing $^1\text{O}_2$ -signalling, which otherwise might be difficult to detect due to the dominant signal(s) originating in PET. The GUN4 protein involved in MgCh function (Supplementary Fig. 1) and signalling degrades upon Proto accumulation¹⁹. However, *chLD-1* overexpressing GUN4 showed higher GUN4 content than *chLD-1*, while it retained the chlorophyll-free phenotype¹⁹. Additionally, *chLD-1/GUN4* demonstrated higher expression of *GLUTATHIONE PEROXIDASE 5* (*GPX5*) and higher tolerance to $^1\text{O}_2$ than *chLD-1*¹⁹. Thus, to minimize the GUN4-deficient phenotype and to maintain high and stable $^1\text{O}_2$ -inducibility of *GPX5* expression, *chLD-1/GUN4* instead of *chLD-1* was used as the receiver strain for the gene construct that allowed us to monitor $^1\text{O}_2$ -signalling. The gene construct introduced into the *chLD-1/GUN4* genome consisted of the promoter region of the *GPX5* gene fused to the promoterless *ARYLSULFATASE 2* gene (*ARS2*). *GPX5* was shown to be specifically induced by $^1\text{O}_2$ in *C. reinhardtii*^{20,24}, while the *ARS2* activity can be assessed by the enzymatic assay²⁵. The resulting *GPX5-ARS2* gene construct was shown previously to be an effective reporter to study $^1\text{O}_2$ -signalling^{15,24,26}. Following introduction of *GPX5-ARS2*, transformant strain showing high inducibility of *GPX5-ARS2* in response to $^1\text{O}_2$ was named *signalling Reporter* (*sigRep*) and was subjected to further studies.

Subsequent random insertional mutagenesis of *sigRep*, followed by a screening for decreased *GPX5-ARS2* expression identified mutants with impaired $^1\text{O}_2$ -signalling. To reflect the impairment in $^1\text{O}_2$ -dependent signalling, these mutants were named *genomes uncoupled Singlet Oxygen Signalling* (*gunsOS*). The *gunsOS1* mutant was selected for further analysis. Although employment of the Proto-accumulating mutant as the background strain provides advantage in studying $^1\text{O}_2$ -signalling, it also results in certain limitations, e.g. lack of chlorophyll enforces heterotrophic growth, alters nuclear gene expression and metabolism. Thus, due to the character of the background strain, phenotype of *gunsOS1* was primarily compared with the parental *sigRep*, instead of the chlorophyll-synthesising WT.

The lack of the retrograde response to $^1\text{O}_2$ in *gunsOS1* was verified by decreased expression of *GPX5*, as well as *SAK1*, *MBS*, and *PSBP2* compared with *sigRep*. The causal mutation in *gunsOS1* was found in a gene annotated as *TREHALOSE 6-PHOSPHATE PHOSPHATASE* (hereafter *TSPP1*). Besides clear impairment in $^1\text{O}_2$ -signalling, mutation in *TSPP1* also resulted in accumulation of trehalose 6-phosphate (Tre6P) in *gunsOS1* compared with *sigRep* and WT. Therefore, *TSPP1* is the first confirmed phosphatase acting on Tre6P in *C. reinhardtii* and in fact the first enzyme with a confirmed function in trehalose metabolism in this organism. Our data indicate that accumulation of Tre6P, alternatively the lack of the *TSPP1* protein, causes changes to the expression of genes involved in several metabolic pathways. However, Tre6P or *TSPP1* are rather

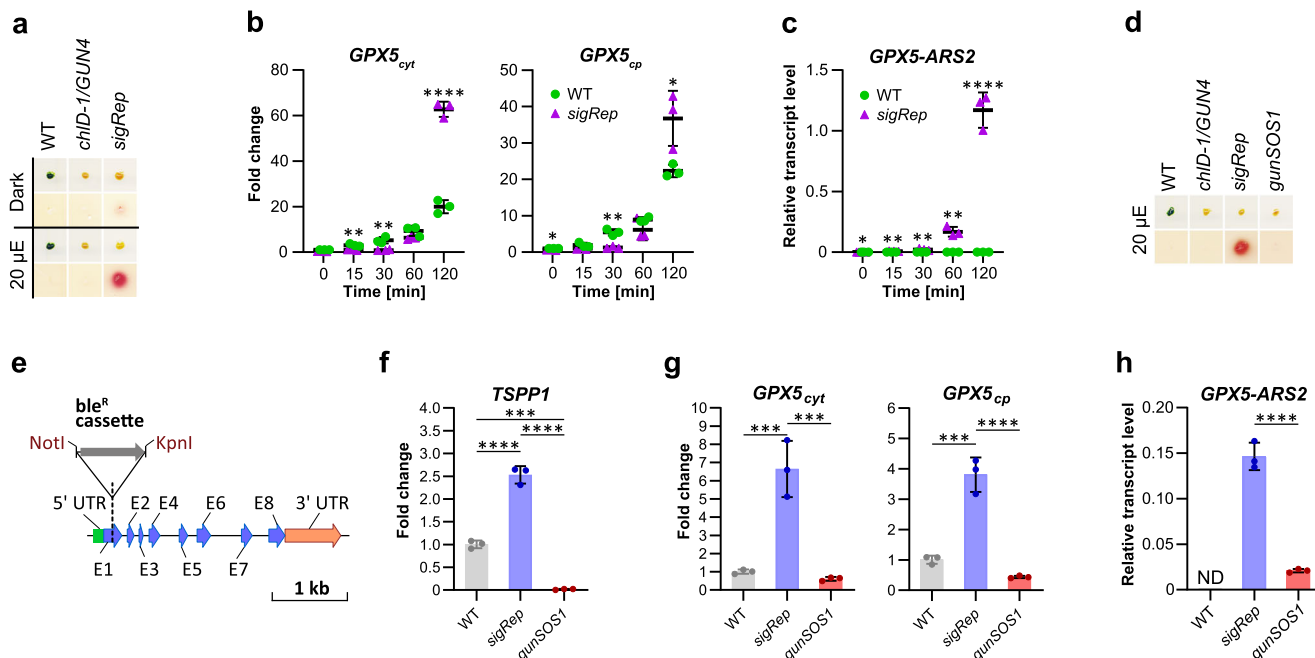


Fig. 1 Generation and initial characterisation of the mutant impaired in $^1\text{O}_2$ -signalling. **a** Arylsulfatase (ARS2) assay for selection of the strain expressing *GPX5-ARS2* reporter gene in a $^1\text{O}_2$ -inducible manner. The mutant selected for further applications was named *sigalling Reporter* (*sigRep*). WT and *chID-1/GUN4* do not carry *GPX5-ARS2* and were used as negative controls in ARS2 assay. **b** Expression kinetics of cytosolic (*GPX5_{cyt}*) and chloroplast *GPX5* (*GPX5_{cp}*) in *sigRep* compared to WT upon exposure to light; the values were calculated as a fold change normalised to WT in dark ($2^{-\Delta\Delta\text{Ct}}$, WT = 1). **c** Expression of *GPX5-ARS2* in *sigRep* positively correlates with time of exposure to light. WT was used as a negative control. **d** ARS2 activity assay following mutagenesis of *sigRep*. Screen was performed to identify mutants not expressing *GPX5-ARS2* compared to *sigRep* in the same conditions. The mutant selected for further applications was named *genomes uncoupled Singlet Oxygen Signalling 1* (*gunSOS1*). WT and *chID-1/GUN4* were used as negative controls. **e** *TSPP1* (Cre12.g497750) gene model. The insertion (*ble^R*) was identified in the first exon of 3241 bp *TSPP1*. **f** Expression of *TSPP1* in *gunSOS1* compared to *sigRep*. **g** Expression of *GPX5_{cyt}* and *GPX5_{cp}* in *gunSOS1* compared to *sigRep*. **h** Expression of *GPX5-ARS2* in *gunSOS1* compared to *sigRep*; WT was used as a negative control (ND, not detectable). For **f–h** (*TSPP1*, *GPX5_{cyt}*, *GPX5_{cp}*, and *GPX5-ARS2*) mRNA was determined 2 h after transfer from dark to light. Transcript analyses were performed by qRT-PCR on biological triplicates, values were calculated either as a fold change ($2^{-\Delta\Delta\text{Ct}}$; normalised to the mean of $\text{Ct}_{\text{exp}} - \text{Ct}_{\text{ref}}$ of WT) or relative transcript level (normalised against a reference gene, calculated as $2^{\Delta\text{Ct}}$). For **b** and **c**, horizontal bars represent the calculated mean ($n = 3$), vertical error bars represent calculated $\pm\text{SD}$; significant differences were calculated using two-tailed Student's *t*-test and are indicated by asterisks (non-significant not shown), * $P < 0.05$, ** $P < 0.01$, *** $P < 0.001$, and **** $P < 0.0001$. For **f–h**, error bars indicate calculated $\pm\text{SD}$; one-way ANOVA, pair-wise comparison with the Tukey's post-hoc test (non-significant not shown), * $P < 0.05$, ** $P < 0.01$, *** $P < 0.001$, and **** $P < 0.0001$.

intermediates than the primary cause of the impaired $^1\text{O}_2$ -signalling. Here, using a combination of genetics, gene expression and metabolic phenotypes, we reveal a complex interaction between chloroplast, mitochondria and cytosol in $^1\text{O}_2$ signal transmission to the nucleus.

Results

Forward genetics screen to identify components of the $^1\text{O}_2$ -signalling. To generate a mutant impaired in $^1\text{O}_2$ -dependent signalling, we first created a reporter strain in a known $^1\text{O}_2$ -generating mutant, which was subsequently subjected to mutagenesis. The *GPX5-ARS2* reporter construct (Supplementary Fig. 2) was introduced into the genome of *chID-1/GUN4* to express the ARS2 protein in a $^1\text{O}_2$ -dependent manner, and the transformants were tested for the enzymatic activity of ARS2. The reporter strain, which showed the lowest ARS2 activity in darkness and the highest activity in light was named *sigalling Reporter* (*sigRep*; Fig. 1a) and was used in further applications. Expression kinetics of the cytosolic (*GPX5_{cyt}*) and chloroplast (*GPX5_{cp}*) version of *GPX5*²⁷; Fig. 1b), as well as the *GPX5-ARS2* construct (Fig. 1c) were examined by quantitative Real-Time PCR (qRT-PCR) upon transfer from dark to light. As expected, higher induction of *GPX5_{cp}* and *GPX5_{cyt}* were observed upon light illumination in *sigRep* compared with WT (Fig. 1b). Induced

GPX5-ARS2 expression in *sigRep* in the light (Fig. 1c) confirmed the results obtained in the ARS activity assay (Fig. 1a) and a suitability of the *sigRep* reporter strain for further applications.

Subsequently, a random mutagenesis was performed on *sigRep* using bleomycin resistance cassette (*ble^R*) as an insert, followed by screening to isolate strains with lower or undetectable ARS2 activity in the light compared with *sigRep*, and thus, possibly disrupted $^1\text{O}_2$ -dependent signalling. Screen of 804 transformants allowed us to isolate nine *gunSOS* mutants. The relatively high number of the obtained mutants with a desired $^1\text{O}_2$ -signalling phenotype might be indicative of the multiple components involved or affecting $^1\text{O}_2$ -signalling and the response to photooxidative stress. These components may be key elements of the signalling pathways alternative to the dominant ROS-signalling originating in PET, or may constitute a part of it in an orchestrated complex network of the signalling pathways, which function becomes more apparent only in artificially generated chlorophyll- and PET-deficient conditions.

The *gunSOS1* mutant (Fig. 1d) was selected for further analysis. Mutant impaired in $^1\text{O}_2$ -signalling showed similar Proto accumulation in light compared with *sigRep* and *chID-1/GUN4* (Supplementary Fig. 3), which eliminated the possibility that spurious mutations in *gunSOS1*, which may have been introduced during mutagenesis, resulted in reduced content of this

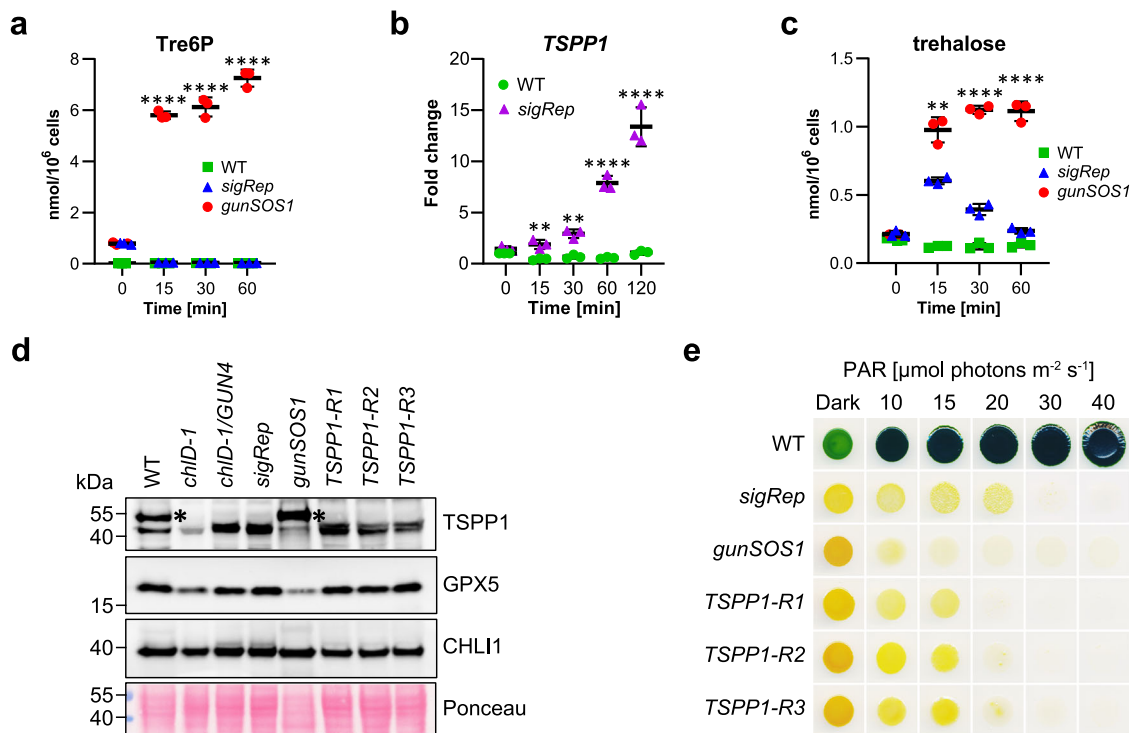


Fig. 2 *C. reinhardtii* TSPPI is a functional phosphatase induced during photooxidative stress. **a** Kinetics of Tre6P accumulation in *gunSOS1* compared to *sigRep* and WT upon transfer from dark to light. **b** Kinetics of TSPPI expression upon transfer from dark to light in *gunSOS1* compared to WT indicated inducibility by photooxidative stress rather than light; the values were calculated as a fold change normalised to WT in dark ($2^{-\Delta\Delta C_t}$, WT = 1). **c** Higher content of trehalose in *gunSOS1* compared to *sigRep* and WT upon transfer from dark to light may be resulting from the possible phosphatase activity of TSPPI, which was not determined in the present study. **d** Immunoblot analysis of TSPPI (calculated MW of 42 kDa) and GPX5 content in *gunSOS1* compared to *sigRep* and strains rescued with the wild-type copy of TSPPI. The CHL11 content was used as a loading control. The unspecific immunoreaction is indicated by an asterisk. **e** Light sensitivity examination showed that the strains with rescued 1O_2 -signalling have an increased tolerance to light compared with *gunSOS1*. Experiments in (a–c) were performed in biological triplicates ($n = 3$), horizontal bars represent the calculated mean, vertical error bars represent \pm SD. The pair-wise statistical analyses in a and c were performed only for *gunSOS1* relative to *sigRep*, the metabolites for photosynthetic WT are shown as a reference; in b *sigRep* is compared to WT. Significant differences were calculated using two-tailed Student's *t*-test and are indicated by asterisks (non-significant not shown), * $P < 0.05$, ** $P < 0.01$, *** $P < 0.001$, and **** $P < 0.0001$.

photosensitizer. Because in our system Proto is considered as the main source of 1O_2 , a lower levels of this ROS in *gunSOS1* compared with *sigRep* would not be expected.

The ble^R insertion in *gunSOS1* was located in the first exon of TSPPI (locus Cre12.g497750) in the JGI portal (Department of Energy Joint Genome Institute, <https://phytozome-next.jgi.doe.gov>, v13, genome v5.6; Fig. 1e). The TSPPI transcript abundance was determined in *gunSOS1* and compared with *sigRep* by qRT-PCR using primers annealing to the coding sequence upstream of the insertion site. At 2 h after transfer from dark to light, TSPPI mRNA content increased 2.5-fold in *sigRep* compared with WT, while it was nearly absent in *gunSOS1* (Fig. 1f). Expression of GPX5_{cyt} and GPX5_{cp} was about 11 and 9 times lower in *gunSOS1* compared with *sigRep*, respectively (Fig. 1g). The transcript abundance for GPX5-ARS2 was 7 times lower in *gunSOS1* than in *sigRep* (Fig. 1h), and explains undetectable ARS2 activity in the 1O_2 -signalling mutant (Fig. 1d).

***C. reinhardtii* TSPPI is a functional Tre6P phosphatase.** While *gunSOS1* is clearly impaired in 1O_2 -signalling, it was necessary to determine the primary phenotype caused by the mutation in TSPPI. The content of Tre6P in *sigRep* and *gunSOS1* was determined by anion-exchange high performance liquid chromatography coupled to tandem mass spectrometry (LC-MS/MS). Tre6P accumulation increased in *gunSOS1* upon exposure to light in a time-dependent manner, while it decreased in *sigRep*

(Fig. 2a). In photosynthetic WT, Tre6P content remained low throughout the entire course of the experiment (Fig. 2a). Accumulation of Tre6P in *gunSOS1* indicates that *C. reinhardtii* TSPPI is a functional phosphatase dephosphorylating Tre6P to trehalose. Subsequently, TSPPI expression was found to be induced in the light in *sigRep*, but not in the WT, indicating its inducibility by photooxidative stress rather than light (Fig. 2b). Mutation of the TSPPI gene would be expected to decrease dephosphorylation of Tre6P and lower trehalose content, but we also observed accumulation of trehalose in *gunSOS1* compared with *sigRep* and WT (Fig. 2c). This apparent discrepancy could be explained by the existence of another enzyme in *C. reinhardtii* with possible Tre6P phosphatase activity, in combination with higher levels of Tre6P. However, this hypothesis was not verified (see the Discussion section).

Rescue of the TSPPI deficiency in *gunSOS1* was performed with the isolated genomic DNA fragment carrying the WT TSPPI gene. Several independent transformants showed rescued 1O_2 -signalling, which was indicated by the GPX5-ARS2 expression determined in the ARS assay, and data from three representative strains are shown in Supplementary Fig. 4a. The analysed rescued strains also showed increased GPX5_{cp} transcript content compared with *gunSOS1* (Supplementary Fig. 4b). A peptide-specific antibody for TSPPI was produced to compare the protein content in *gunSOS1* to strains showing 1O_2 -dependent signalling. A faint immune signal of ~43 kDa was detected in *gunSOS1* and *chID-1*, but two narrow bands were seen in *chID-1/GUN4*, *sigRep* and the

TSPP1-rescued strains (Fig. 2d). WT and *gunSOS1* showed an additional unspecific immunoreaction with protein of ~53 kDa. As expected, the GPX5 protein content was lower in *gunSOS1* compared with *sigRep* (Fig. 2d), which correlated with qRT-PCR results on GPX5 transcript levels (Fig. 1g). While higher sensitivity to light was recorded in *gunSOS1* compared with the *sigRep* background strain (Fig. 2e), in agreement with a higher sensitivity or impaired acclimation to $^1\text{O}_2$. Strains with rescued $^1\text{O}_2$ -signalling, *TSPP1-R1*, *-R2*, and *-R3*, showed increased content of GPX5 (Fig. 2d) and subsequently higher tolerance to light compared with *gunSOS1* (Fig. 2e).

The *gunSOS1* mutant shows altered metabolism compared with *sigRep*. In *A. thaliana* and other angiosperms, Tre6P functions as a sucrose signal and homeostatic regulator of sucrose metabolism^{28,29}, which links plant growth and development to the availability of sucrose³⁰, reviewed in³¹. To determine the effect of accumulated Tre6P on metabolism in *C. reinhardtii*, we performed comparative metabolite profiling of *gunSOS1* and *sigRep* (Supplementary Table 1), which revealed a relatively wide range of variation. In our metabolite analyses we focused on the differences between *gunSOS1* and *sigRep*. However, the content of the same metabolites was also determined in WT, which was used only as a reference for non-photosynthetic *gunSOS1* and *sigRep*. Aside from Tre6P and trehalose, 11 out of 27 analysed metabolites showed significantly increased content in *gunSOS1* compared with *sigRep* in the light (Supplementary Fig. 5a). By means of the MetaboAnalyst 5.0 portal (<https://www.metaboanalyst.ca>) these metabolites were assigned to the metabolic processes in the cell. A hypergeometric test indicated the most affected metabolic pathways, i.e. the TCA cycle, pyruvate metabolism, and starch and sucrose metabolism (Supplementary Fig. 5b and Supplementary Table 2). Eight metabolites showed significantly decreased content in *gunSOS1* compared with *sigRep* (Supplementary Fig. 6a), with the highest impact (MetaboAnalyst 5.0) on fructose and mannose metabolism, amino sugar and nucleotide sugar metabolism, and starch and sucrose metabolism (Supplementary Fig. 6b and Supplementary Table 3). Metabolites, which did not show a significant change in *gunSOS1* compared with *sigRep* are presented in Supplementary Fig. 7. The map-overview of the selected metabolic pathways with depicted metabolites that showed different content, or were not changed, in *gunSOS1* relative to *sigRep* is presented in Fig. 3.

Starch content was determined in *gunSOS1* and compared with *sigRep*, because of changes in several intermediates of starch and sucrose metabolism (Supplementary Figs. 5b and 6b). Indeed, *gunSOS1* accumulated only 60% of the starch content of *sigRep* when the strains were grown in acetate-supplemented media (TAP, Supplementary Fig. 6c). Both *sigRep* and *gunSOS1* are obligate heterotrophs. *SigRep* contained less starch after transfer from TAP and cultivation in TP for 48 h, whereas the starch content of *gunSOS1* was essentially unchanged (Supplementary Fig. 6c), indicating that there was net degradation of starch in *sigRep* but not in *gunSOS1*. Starch formation is strongly induced during nitrogen (N) deprivation³². The *sigRep* cells did not increase starch reserves after 3 days in N-deficient medium, suggesting that starch accumulation had already reached its maximum under non-stress conditions. The starch content in *gunSOS1* deprived of N did increase by 50% and was similar to the content in *sigRep* (Supplementary Fig. 6c). We conclude that *sigRep* accumulates high levels of starch as a consequence of the *chLD-1/GUN4* genetic background and that the accumulation of Tre6P represses this response in *gunSOS1* leading to a lower accumulation of starch. The *gunSOS1* cells are still capable of responding to the N-deprivation stress and accumulating starch

despite disturbed metabolism. Starch degradation on the other hand, is compromised in *gunSOS1*, which could indicate a general impairment of catabolic processes or a defect in sensing carbon limitation.

Increased Tre6P content alters metabolism in *C. reinhardtii* via transcriptional changes. To determine the extent to which chloroplast retrograde signalling is affected in *gunSOS1*, we performed comparative RNA-sequencing (RNA-seq) of the transcriptomes of *gunSOS1* and *sigRep* upon transfer from dark to light. The analysis showed that 8120 genes were expressed in both strains, but 1377 and 1087 additional genes were uniquely expressed in *gunSOS1* and *sigRep*, respectively (Fig. 4a, detailed listing can be found in Supplementary Data 1). Furthermore, differential gene expression analysis showed that the transcript contents of 1606 genes and 1706 genes were lower or higher, respectively, in *gunSOS1* compared with *sigRep* (Supplementary Data 2).

Based on the KEGG ontology (<http://www.kegg.jp/>) several genes associated with metabolic pathways were down- or up-regulated (Fig. 4b) in *gunSOS1* compared with *sigRep* (Supplementary Data 3). Given the strong overlap between differentially expressed genes and corresponding pathway intermediates, we hypothesized that the altered metabolism can be directly explained by altered gene expression. To decipher a complex correlation between altered signalling, gene expression and metabolism, accumulation or deficiency in metabolites from given pathway(s) was correlated with altered gene expression in *gunSOS1* compared with *sigRep*. Fumarate and aconitate will be described in more detail, as representative examples of the metabolites showing respectively increased or decreased content in *gunSOS1* compared with *sigRep*.

KEGG enrichment of the RNA-seq data indicated increased expression of the gene encoding fumarate hydratase class II (FUM2, Enzyme Commission (EC) Number 4.2.1.2, Cre01.g020223) in *gunSOS1* compared with *sigRep*. FUM is responsible for reversible stereospecific interconversion of malate to fumarate. However, specific isoforms of this protein act in defined pathways and may favour one direction over the other depending on the subcellular localisation and environment³³. The mitochondrial isoform catalyses hydration of fumarate to L-malate in the TCA cycle, while the cytosolic form catalyses dehydration of L-malate to fumarate^{34,35}. Two isoforms exist in *C. reinhardtii*, FUM1 encoded in locus Cre06.g254400 and FUM2. Based on the predicted subcellular localisation (PredAlgo; <http://lobosphaera.ibpc.fr/cgi-bin/predalgotdb2.perl?page=main>), FUM1 localises to the mitochondria, while FUM2 is assigned to the “other” compartment and is likely to be a cytosolic protein. Pathway (KEGG) diagrams for the TCA cycle and pyruvate metabolism can be found in Supplementary Fig. 8, showing integration of metabolite, RNA-seq and qRT-PCR data. Comparison of the transcriptomes of *gunSOS1* and *sigRep* also indicated increased expression of the *FUMARYLACETOACETASE* gene (locus Cre17.g732802, EC 3.7.1.2) involved in tyrosine catabolism. Fumarylacetoacetase catalyses hydrolysis of 4-fumarylacetoacetate to acetoacetate and fumarate (Supplementary Fig. 9). Increased expression of genes encoding FUM2 and fumarylacetoacetase could explain accumulation of fumarate in *gunSOS1* compared with *sigRep*.

Aconitate deficiency in *gunSOS1* compared with *sigRep* can be explained by transcriptional downregulation of *ACONITATE HYDRATASE* (*ACH1*, Cre01.g042750, EC 4.2.1.3). *ACH1* interconverts citrate and isocitrate, via cis-aconitate, in the TCA cycle (Supplementary Fig. 10) and is also involved in glyoxylate and dicarboxylate metabolism. At equilibrium, the reactants of the

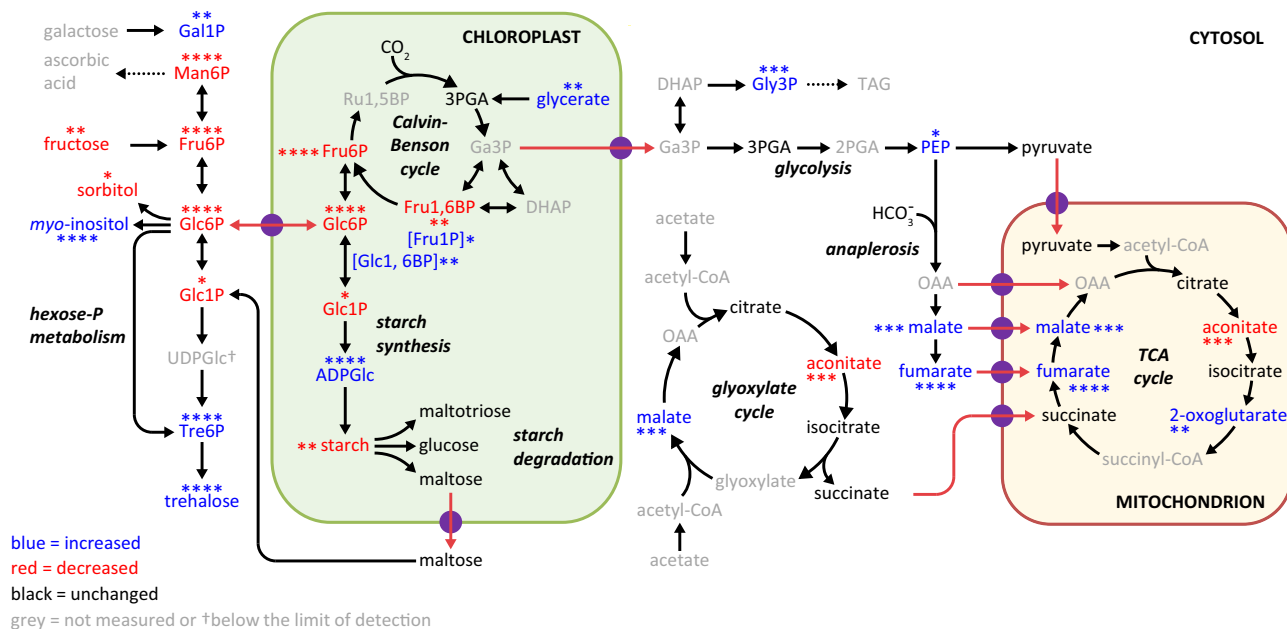


Fig. 3 The overview of the selected metabolic pathways in *gunSOS1* compared with *sigRep*. The map was constructed based on the measured metabolites presented in Supplementary Figures 5a, 6a, and 7. Metabolites increased in *gunSOS1* compared to *sigRep*: fumaric acid (fumarate), oxoglutaric acid (2-OG), myo-inositol, ADP-glucose (ADPGlc), galactose 1-phosphate (Gal1P), fructose 1-phosphate (Fru1P), alpha-D-glucose 1,6-bisphosphate (Glc1, 6BP), glycerol 3-phosphate (Gly3P), phosphoenolpyruvic acid (PEP), and L-malic acid (malate). Metabolites decreased in *gunSOS1* compared to *sigRep*: cis-aconitic acid (aconitate), mannose 6-phosphate (Man6P), glucose 6-phosphate (Glc6P), D-fructose (fructose), fructose 6-phosphate (Fru6P), glucose 1-phosphate (Glc1P), fructose 1,6-bisphosphate (Fru1, 6BP), and sorbitol. Metabolites that did not show significant difference in *gunSOS1* relative to *sigRep*: D-glucose (glucose), D-maltose (maltose), maltotriose, citric acid (citrate), isocitric acid (isocitrate), pyruvic acid (pyruvate), succinic acid (succinate), and 3-phosphoglyceric acid (3PGA). The colour-coding is shown in the legend. Measurements were performed in biological triplicates ($n = 3$); significant differences were calculated using two-tailed Student's *t*-test. The maximal significant differences from any time point in light (Supplementary Figures 5a and 6a) are indicated by asterisks, * $P < 0.05$, ** $P < 0.01$, *** $P < 0.001$, and **** $P < 0.0001$.

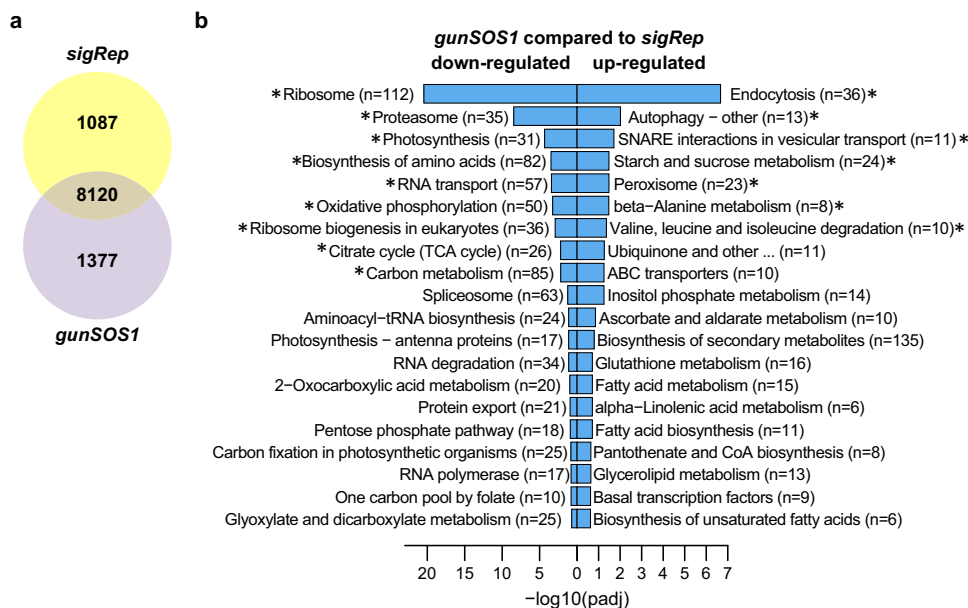


Fig. 4 Transcriptome analysis based on RNA-seq. a Venn diagram showing number of genes expressed in *gunSOS1* and *sigRep* (8120), or uniquely expressed in *gunSOS1* (1377) or in *sigRep* (1087). **b** Pathway enrichment analysis (KEGG, <http://www.kegg.jp/>) based on the differentially expressed genes (RNA-seq). Effect on metabolic processes is sorted by the *P* value. Asterisks in b indicate the core (significant) enrichment.

ACH1 reaction are present in the following ratio: 91% citrate, 6% isocitrate and 3% aconitate. With the smallest pool of the three tricarboxylic acids, fluctuations in the level of aconitate are expected to be more pronounced compared with the other

metabolites involved, especially citrate, whose content was similar in *gunSOS1* and *sigRep* in the light (Supplementary Fig. 7). Taken together, our data indicate that altered fumarate and aconitate content in *gunSOS1* compared with *sigRep* can be explained by

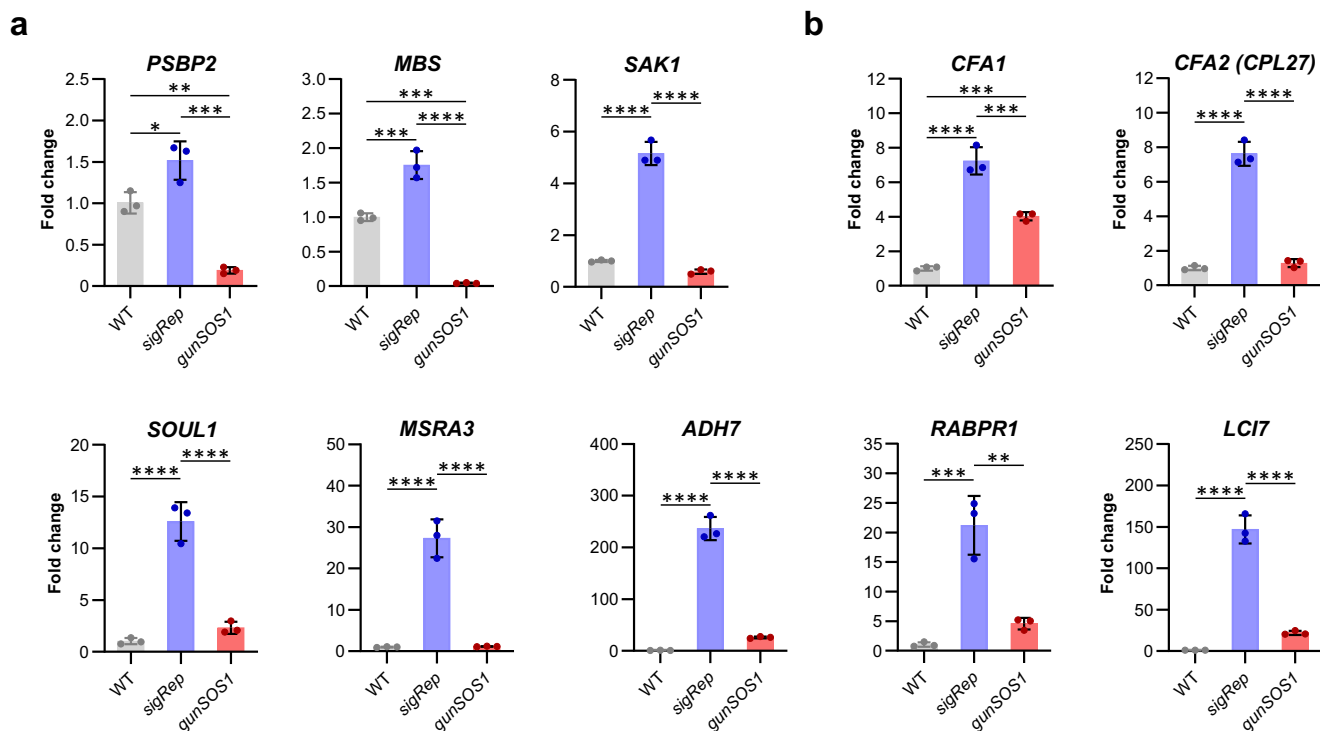


Fig. 5 The qRT-PCR analysis of gene expression in *gunSOS1* compared to *sigRep*. **a** Expression of genes encoding protein components previously associated with the chloroplast retrograde signalling involving $^1\text{O}_2$, *PSBP2*¹⁵, *MBS*¹⁷, and *SAK1*¹⁶. **b** Transcript levels of the selected genes showing attenuated expression in *gunSOS1* compared to *sigRep* in the context of the *SAK1*-transcriptome¹⁶, genes description in the text. Experiments were performed in biological replications ($n = 3$); results are presented as a fold change ($2^{-\Delta\Delta\text{Ct}}$, normalised to the mean of $\text{Ct}_{\text{exp}} - \text{Ct}_{\text{ref}}$ of WT); the error bars represent calculated \pm SD. Significant differences were calculated using one-way ANOVA, pair-wise comparison with the Tukey's post-hoc test (non-significant not shown), * $P < 0.05$, ** $P < 0.01$, *** $P < 0.001$, and **** $P < 0.0001$.

altered expression of genes encoding enzymes involved in key metabolic processes affecting those metabolites.

Impaired $^1\text{O}_2$ -signalling in *gunSOS1* correlates with decreased expression of *PSBP2*, *MBS*, and *SAK1*. The *PSBP2*¹⁵, *MBS*¹⁷, and *SAK1*¹⁶ proteins are required for $^1\text{O}_2$ -induced chloroplast retrograde signalling in *C. reinhardtii*. Therefore, we determined the transcript levels of *PSBP2*, *MBS*, and *SAK1*, which were 8-, 9-, and nearly 41-fold lower, respectively, in *gunSOS1* compared with *sigRep* (Fig. 5a). Decreased expression of *SAK1* in *gunSOS1* prompted us to compare transcript levels of selected $^1\text{O}_2$ -responsive genes between *gunSOS1* and the *sak1* mutant, reported in Wakao et al.¹⁶ *SAK1* is a key regulator of the gene expression response and its knockout abolishes acclimation response to $^1\text{O}_2$ ¹⁶. The involvement of *SAK1* in $^1\text{O}_2$ -signalling was determined following treatment with rose bengal¹⁶, which produces $^1\text{O}_2$ in the light, while in *gunSOS1* the main source of $^1\text{O}_2$ is endogenously accumulating Proto (Supplementary Fig. 3). Nevertheless, based on our qRT-PCR analysis, all tested genes had the same reduced inducibility in *gunSOS1* compared with *sigRep* (Fig. 5b), as it was observed in *sak1* compared with its corresponding WT following $^1\text{O}_2$ -exposure¹⁶. Among the genes that were down-regulated in both *gunSOS1* (Fig. 5b) and *sak1*¹⁶ were two *CYCLOPROPANE FATTY ACID SYNTHASES*, *CFA1* and *CFA2 (CPLD27)*, involved in lipid and sterol metabolism, as well as the gene encoding *SOUL1* heme-binding protein (Fig. 5b). It is noteworthy that attenuated expression of both *CFA1* and *CFA2*, as well as *SOUL1*, was also observed in studies on a *gpx5* mutant³⁶. Furthermore, in agreement with the *sak1* phenotype presented in ref. ¹⁶, *gunSOS1* also showed decreases in transcript content of *PEPTIDE METHIONINE SULFOXIDE REDUCTASE*

(*MSRA3*), *ALCOHOL DEHYDROGENASE (ADH7)*, *RETINALDEHYDE BINDING PROTEIN-RELATED (RABPR1)*, and *LOW-CO₂-INDUCIBLE PROTEIN 7 (LCI7)* (Fig. 5b). Thus, there is an overlap between the phenotypes of *gunSOS1* and *sak1*¹⁶ with respect to their attenuated expression of genes induced during elevated $^1\text{O}_2$ (Fig. 5b).

Altered metabolite content affects $^1\text{O}_2$ -signalling. We hypothesized that at least some of the metabolites showing increased or decreased content in *gunSOS1* compared with *sigRep*, attenuate or propagate $^1\text{O}_2$ -signalling, respectively. To test this hypothesis, we undertook the most straight-forward approach by application of selected metabolites individually, at pre-determined sub-lethal concentrations. Addition of metabolites was followed by incubation in light to induce $^1\text{O}_2$ -generation by Proto and subsequent examination of the *GPX5* expression as readout for functional $^1\text{O}_2$ -signalling. Selection of the metabolites to be tested was mostly based on their involvement or effect on the intracellular signalling processes reported in the literature.

Concerning selected metabolites accumulating in *gunSOS1* relative to *sigRep* exposed to $^1\text{O}_2$ -stress (Supplementary Fig. 5a), fumarate is a well-recognised oncometabolite in mammalian cells³⁷. 2-oxoglutarate lies at the intersection between the carbon and nitrogen metabolic pathways and it was shown to regulate (together with glutamine) expression of *NITRATE REDUCTASE* in *Nicotiana tabacum*³⁸. Other studies also suggested 2-oxoglutarate playing a role as a signal metabolite in plants^{39,40}. Myo-inositol is a building block for several molecules involved in signalling, such as myo-inositol (1,4,5)trisphosphate or phosphatidylinositol (4,5)bisphosphate (reviewed in⁴¹). Exogenously provided fumarate, 2-oxoglutarate, and myo-inositol, always

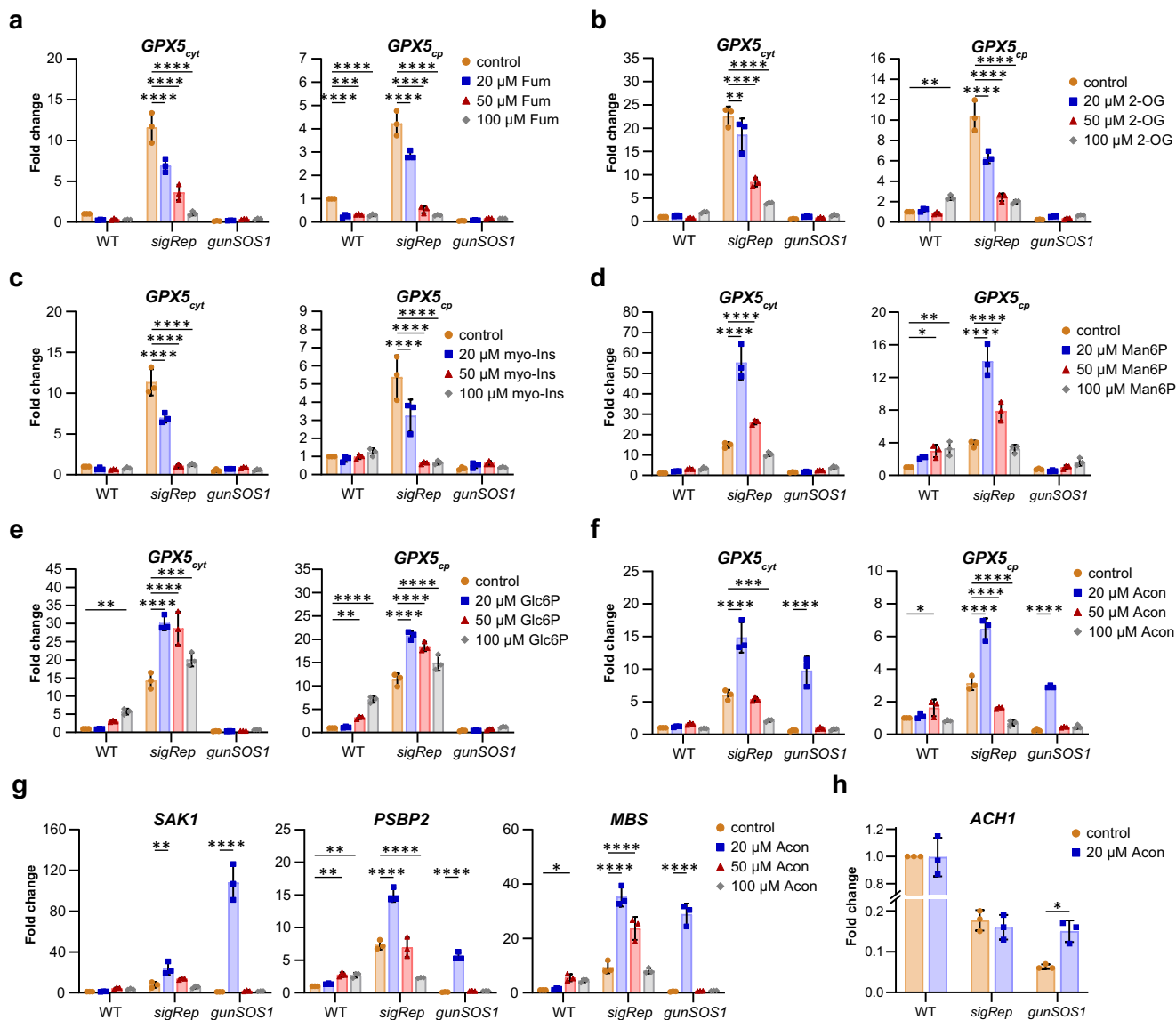


Fig. 6 Effect of selected metabolites applied exogenously on $^1\text{O}_2$ -signalling inducing GPX5_{cyt} or GPX5_{cp} expression. **a** Fumarate (Fum) significantly ($P < 0.0001$) decreased the GPX5 expression in *sigRep* in concentration-dependent manner. **b** 2-oxoglutarate (2-OG) significantly ($P < 0.0001$) decreased expression of GPX5 in *sigRep*. **c** Myo-inositol (myo-Ins) significantly ($P < 0.0001$) decreased expression of GPX5 in *sigRep*. **d** Mannose 6-phosphate (Man6P) at 20 μM and 50 μM increased the GPX5 expression in *sigRep*. **e** Application of glucose 6-phosphate (Glc6P) always significantly ($P < 0.0001$) increased the GPX5 expression in *sigRep*. **f** Aconitate (Acon) at 20 μM concentration rescued GPX5 expression in *gunSOS1* and increased GPX5 expression in *sigRep*. Statistical analysis showed that 20 μM aconitate significantly ($P \leq 0.0001$) affected GPX5 expression in *gunSOS1* and *sigRep*. **g** Transcripts of proteins necessary for the $^1\text{O}_2$ -signalling, *PSBP2*, *MBS*, and *SAK1*, significantly ($P < 0.01$) increased upon treatment with 20 μM aconitate. **h** Increase in *ACH1* expression upon treatment with aconitate, compared to *sigRep*. The qRT-PCR experiments were performed in biological replications ($n = 3$); results are presented as a fold change normalised to untreated WT ($2^{-\Delta\Delta\text{Ct}}$, WT = 1); the error bars represent calculated $\pm\text{SD}$. For a-g significant differences were calculated using two-way ANOVA with Dunnett's multiple comparison test and are indicated by asterisks (non-significant changes are not shown for clarity). For h significant change was calculated using multiple *t*-test comparing treated to untreated cells of a given strain. * $P < 0.05$, ** $P < 0.01$, *** $P < 0.001$, and **** $P < 0.0001$. Detailed statistical analyses are presented in Supplementary Tables 4-19.

significantly (detailed report from two-way ANOVA analyses is presented in Supplementary Tables 4-9) attenuated expression of GPX5 in a concentration-dependent manner in *sigRep*, with no change in *gunSOS1* and WT, relative to their respective non-treated controls (Fig. 6a-c). Among the selected metabolites, which showed decreased content in *gunSOS1* relative to *sigRep* (Supplementary Fig. 6a), were mannose 6-phosphate, glucose 6-phosphate, and aconitate. The effect on $^1\text{O}_2$ -signalling of exogenously applied sugar phosphates was tested because of their known inhibitory effect on sucrose-non fermenting (SNF)-related

protein kinase 1 (SnRK1) in plants^{42,43}. Application of mannose 6-phosphate and glucose 6-phosphate had a similar effect on GPX5 expression in *sigRep*, with significant increase at 20 and 50 μM . However, no effect on GPX5 mRNA could be detected in *gunSOS1* (Fig. 6d, e, Supplementary Tables 10-13). Based on the literature, aconitate was never implicated in the signalling and it was selected randomly. Nevertheless, application of 20 μM aconitate significantly ($P < 0.0001$, Supplementary Tables 14 and 15) increased expression of GPX5 in *gunSOS1* and even further in *sigRep* compared with untreated cells, but 50 and 100 μM had a

quenching effect on the *GPX5* expression in *sigRep* (Fig. 6f). This indicates that aconitate up to a certain threshold concentration promotes $^1\text{O}_2$ signalling in otherwise aconitate-deficient *gunSOS1*. This result encouraged us to study the effect of exogenously applied aconitate further.

Subsequently, we determined the expression of *SAK1* upon feeding *gunSOS1* and *sigRep* with aconitate. Exogenous application of aconitate at 20 μM increased *SAK1* transcript abundance in *gunSOS1* >120 times compared with the untreated *gunSOS1* control, and exceeded values observed in *sigRep* subjected to the same treatment by a factor of 5 (Fig. 6g). Due to the increased *SAK1* expression in *gunSOS1* upon feeding with aconitate, we also determined the expression of *PSBP2* and *MBS* in the same conditions. The *PSBP2* response to aconitate was similar to *SAK1* in terms of the increased expression (Fig. 6g), but with less pronounced dependence on the metabolite concentration compared with *SAK1*. Although 20 μM aconitate increased *PSBP2* expression in *gunSOS1* by a factor of 48 compared to the untreated control, it was still 2.7 times lower compared with *sigRep* subjected to the same treatment (Fig. 6g). Similarly to *SAK1* and *PSBP2*, 20 μM aconitate also increased expression of *MBS* in *gunSOS1*, although values did not exceed those observed in *sigRep* subjected to the same treatment (Fig. 6g). Statistical analyses indicated that the effect of 20 μM aconitate on *SAK1*, *PSBP2* and *MBS* expression in *sigRep* and *gunSOS1*, interaction between mutants and aconitate, as well as the mutant-dependent expression of these genes were always significant ($P < 0.001$, Supplementary Tables 16–18).

The rescued expression of the genes encoding *SAK1*¹⁶, *PSBP2*¹⁵, and *MBS*¹⁷ (Fig. 6g), consequently rescued $^1\text{O}_2$ -signalling and the expression of *GPX5* (Fig. 6f) upon exogenously applied aconitate is intriguing, but the underlying mechanism remains unknown. However, substantial amount of data indicated the key role of aconitase (EC 4.2.1.3) in responses triggered by ROS^{44,45}. The decreased expression of *ACH1* in *gunSOS1* relative to *sigRep* (Supplementary Data 2; Supplementary Fig. 10) does not affect the content of citrate and isocitrate (Supplementary Fig. 7), but only deficiency in aconitase was observed in *gunSOS1* compared with *sigRep* (Supplementary Fig. 6a). Thus, we tested the possibility that exogenously provided aconitate affects expression of *ACH1* in *gunSOS1*. As previously observed (Supplementary Fig. 10b), expression of *ACH1* was lower in *sigRep* compared with WT and it did not change upon treatment with aconitate (Fig. 6h). However, upon application of 20 μM aconitate expression of *ACH1* in *gunSOS1* increased 2.5-fold compared with untreated *gunSOS1* control and reached the levels observed in *sigRep* (Fig. 6h; $P < 0.05$, Supplementary Table 19). This result indicated that aconitate content can also affect expression of *ACH1* and points to possible correlation between aconitase function and $^1\text{O}_2$ -signalling.

Specificity of the $^1\text{O}_2$ -signalling pathway(s) attenuated in *gunSOS1*. The profound effect of accumulating Tre6P on the transcriptome (Fig. 4a, b) and consequently the metabolism of *gunSOS1* (Fig. 3 and Supplementary Figs. 5 and 6) may have been indicative of a general photooxidative stress response being impaired in *gunSOS1*. To determine the specificity of this response, we compared *gunSOS1* and *sigRep* in terms of the expression of selected genes that are known to be induced by various reactive species or conditions causing photooxidative stress other than $^1\text{O}_2$.

Upon H_2O_2 or organic *tert*-butyl hydroperoxide (*t*-BOOH) treatment, Blaby, et al.⁴⁶ observed an increase in the expression of the *MSD3* gene, encoding plastid-localised Mn superoxide dismutase 3. In our studies, we did not observe an increase in

MSD3 transcript in *sigRep* compared with WT (Supplementary Fig. 11a), which shows that *MSD3* expression is not inducible by $^1\text{O}_2$ produced by Proto. However, based on qRT-PCR analysis, a 9-fold increase was observed in *gunSOS1* compared with *sigRep* (Supplementary Fig. 11a, see also RNA-seq in Supplementary Data 2). Upon H_2O_2 or *t*-BOOH treatment, Urzica, et al.⁴⁷ also observed induced expression of genes involved in the glutathione-ascorbate system, *GDP-L-GALACTOSE PHOSPHORYLASE* (*VTC2*) and *DEHYDROSASCORBATE REDUCTASE* (*DHAR1*). Based on our qRT-PCR results, *VTC2* transcript content was not changed in *sigRep* compared with WT, but an increase was observed in *gunSOS1* (Supplementary Fig. 11b and Supplementary Data 2). *DHAR1* expression was also stimulated in *gunSOS1* compared with *sigRep* (Supplementary Fig. 11c and Supplementary Data 2).

Similarly to *sak1* following treatment with rose bengal¹⁶, we observed increased expression of *GLUTATHIONE S-TRANSFERASE* (*GST1*) in *gunSOS1* compared with *sigRep* (Supplementary Fig. 11d and Supplementary Data 2). However, in another study increased expression of *GST1* was shown after treatment with acrolein, which suggests its transcriptional induction by reactive electrophile species (RES)⁴⁸. Acrolein was also shown to induce *FSD1* encoding Fe superoxide dismutase (FeSOD)⁴⁸, which was expressed both in *sigRep* and *gunSOS1* (Supplementary Data 1), and no significant difference could be observed in DEG analysis (Supplementary Data 2) or qRT-PCR (Supplementary Fig. 11e). It can be concluded that, despite impaired $^1\text{O}_2$ -signalling, *gunSOS1* retained the ability to express selectively tested genes, which induction was previously associated with response to other ROS, such as H_2O_2 , organic peroxides, or RES.

Discussion

ROS are formed as a by-product of biological redox reactions⁴⁹ mostly in the mitochondria or chloroplasts^{50,51}. Although excess ROS production can cause oxidative damage to cell components, ROS or the oxidation products play an important role in the signal transduction processes. Different retrograde signalling pathways have been proposed to involve also TBS-intermediates in plants and green algae (reviewed in ref. 52,53). While involvement of Mg-porphyrins in chloroplast retrograde signalling is now excluded^{54,55}, in the present study we have demonstrated that $^1\text{O}_2$ produced by the photosensitizing activity of Proto in the light triggers signalling cascades that alter nuclear gene expression in mutant that endogenously accumulate Proto.

The $^1\text{O}_2$ -induced signalling phenotype in the *gunSOS1* mutant was due to a lesion in the *TSPP1* gene. We demonstrated that *TSPP1* is a functional phosphatase responsible for dephosphorylating Tre6P (Fig. 2a, d). *TSPP1* is the only representative of the classical plant *TPP* gene family in *C. reinhardtii*, contrasting with the large *TPP* gene families in angiosperms⁵⁶. In addition, *C. reinhardtii* has one representative of the class I *TREHALOSE-6-PHOSPHATE SYNTHASE* (*TPS*) family (Cre16.g662350, hereafter *TSPS1*), and two members of the class II *TPS* family (Cre06.g278221, here *TSSP1* and Cre16.g686200, here *TSSP2*). Both class I and class II *TPS* proteins have glucosyltransferase and *TPP*-like domains, but only the class I *TPS* proteins have demonstrated *TPS* activity^{57–59}. *TSPP1* belongs to the haloacid dehalogenase superfamily of proteins and contains the characteristic DXDX(T/V) active site motif –₁₀₇DYDGT₁₁₂– in which the initial Asp residue forms a phospho-acyl intermediate during catalysis⁶⁰. *TSSP1* also contains the complete active site motif (₅₉₂DYDGT₅₉₇), so we cannot exclude the possibility that the *TSSP1* protein in *C. reinhardtii* has a phosphatase activity, which could explain the increased content of trehalose in

gunSOS1 compared with *sigRep* (Fig. 2c). Although the intracellular localisations of these proteins have not been determined experimentally in *C. reinhardtii*, PredAlgo analysis indicated possible localisation of TSPP1 and TSSP1 in mitochondria, while TSPS1 and TSSP2 are likely to be cytosolic proteins, because they were not assigned to any specific organelle.

Correlation between TSPP1 (Fig. 2b) and GPX5 (Fig. 1b, c) expression may be indicating that low Tre6P content is necessary for efficient $^1\text{O}_2$ -signalling. However, the apparent negative effect of accumulating Tre6P or the absence of TSPP1 on $^1\text{O}_2$ -signalling is not direct and involves a complex metabolic reprogramming (Fig. 4a, b) leading to altered metabolite content (Fig. 3 and Supplementary Figs. 5 and 6). Study on the contrasting phenotypes between *A. thaliana* overexpressing bacterial TPS, TPP, or trehalose phosphate hydrolase (TPH) pointed to Tre6P, rather than trehalose, playing a signalling function³⁰. Nevertheless, Tre6P was shown to be highly correlated with sucrose, leading to the proposal that it functions as a signal of sucrose status²⁸. Tre6P was also shown to inhibit starch degradation in *A. thaliana*^{61,62}, which is also true in Tre6P-accumulating *gunSOS1* mutant of *C. reinhardtii* (Supplementary Fig. 6c). However, although our analyses revealed the sensitivity of $^1\text{O}_2$ -dependent retrograde signalling to metabolites, it is less clear if Tre6P or the TSPP1 protein itself, or both, play a direct role in metabolic reprogramming (Fig. 3 and Supplementary Figs. 5 and 6). TPP in *Z. mays* is encoded by RAMOSA3 (RA3) and the *ra3* mutants showed reduced meristem determinacy⁶³, without altering the Tre6P content compared with WT plants⁶⁴. Additionally, a catalytically inactive version of RA3 complemented the *ra3* phenotype, which revealed the “moonlighting” function of TPP, i.e. its function aside from the catalysis of Tre6P dephosphorylation⁶⁴. Subsequent study also demonstrated “moonlighting” function of RA3 in carpel suppression⁶⁵. Rather regulatory than a catalytic function was also proposed for TPP7 in *Oryza sativa*, due to its low activity in vitro and no apparent effect on Tre6P content in knockout mutants of TPP⁷⁶. In either case, although in our study the lack of functional TSPP1 clearly results in accumulation of Tre6P, we cannot exclude that the TSPP1 protein itself is involved in inducing changes to the nuclear gene expression (Fig. 4) and metabolic reprogramming (Fig. 3 and Supplementary Figs. 5 and 6).

Nonetheless, it was demonstrated that Tre6P acts as an inhibitor of SnRK1 in developing tissues and that this is dependent on a so-far unidentified protein factor^{43,67,68}. Tre6P also inhibits the activation of SnRK1 by SnRK1-activating kinases/geminivirus Rep interacting kinases⁶⁹. SnRK1 belongs to the AMPK-SNF1-SnRK family of protein kinases, which is represented in all eukaryotes⁷⁰. In plants, SnRK1 plays a central role in energy and metabolic homeostasis, and is activated during energy deficient conditions caused by stresses like nutrient starvation, pathogen attack, or ROS⁷¹. Baena-González et al.⁷² established approximately 1000 genes as markers of SnRK1 in *A. thaliana*, which indicates an extensive SnRK1-dependent transcriptional reprogramming. In *C. reinhardtii*, involvement of various SnRKs in responses to stress was observed during sulphur^{73,74} and nitrogen deprivation⁷⁵, or cold stress⁷⁶. Genome-wide analysis revealed the existence of 21 genes as potential orthologues of the plant SnRK α , β and $\gamma/\beta\gamma$ subunits in *C. reinhardtii*. It was suggested that the proteins encoded by these genes play the same role in cell survival and stress response in *C. reinhardtii* as SnRKs in land plants⁷⁵.

In analogy to *A. thaliana*, altered SnRKs activity was shown to cause metabolic remodelling also in algae⁷⁶. In our study, if the majority of changes to gene expression observed in *gunSOS1*, relative to *sigRep*, originate from accumulation of Tre6P and not the absence of TSPP1, based on previous studies, this may lead to inhibition of one or more SnRKs (Fig. 7). Our analysis showed that

altered gene expression in *gunSOS1* relative to *sigRep* (Supplementary Figs. 8–10) is directly responsible for altered fumarate and aconitate content in *gunSOS1* compared with *sigRep*. Thus, Tre6P accumulating in *gunSOS1* is not directly involved in $^1\text{O}_2$ -signalling but controls other processes in the cell which affect $^1\text{O}_2$ -signalling more directly (Fig. 7).

We demonstrated that accumulation of fumarate, 2-oxoglutarate, or myo-inositol (Fig. 3 and Supplementary Fig. 5a) is capable of attenuating $^1\text{O}_2$ -signalling (Fig. 6a–c, see also model in Fig. 7). On the other hand, application of mannose 6-phosphate and glucose 6-phosphate had a positive effect on GPX5 expression in *sigRep*, but not in *gunSOS1* (Fig. 6d, e). The mechanism behind individual effect of any of these metabolites on $^1\text{O}_2$ -signalling remains unknown. However, considering the rescue of the $^1\text{O}_2$ -signalling upon treatment with aconitate (Fig. 6f), interplay between fumarate and aconitate content can be hypothesized to play a role in this signalling pathway. Fumarate is associated with development of tumours by competitive inhibition of 2-oxoglutarate-dependent oxygenases, including hypoxia inducible factor (HIF) hydroxylases, leading to stabilisation of HIF and activation of oncogenic HIF-dependent pathways⁷⁷. In fact, accumulation of fumarate in human cells was linked to an aggressive variant of hereditary kidney cancer⁷⁸. In mice, fumarate was also shown to directly modify some proteins by succination of cysteine residues to form 2-succinocysteine derivatives⁷⁹. Succination of three cysteines crucial for iron-sulphur cluster binding was identified in mitochondrial aconitase 2 (ACO2) in a *fumarate hydratase 1* knockout (Fh1KO) mouse embryonic fibroblast (MEF) cell line⁷⁹. Analysis of tryptic peptides derived from ACO2 in Fh1KO MEFs, indicated succination of Cys385. Another tryptic peptide of ACO2 was identified as a mixture of two isomers in Fh1KO MEFs, which showed succination at Cys451 or Cys448⁷⁹. In vitro experiments indicated that succination of these cysteine residues in ACO2 leads to its inhibition⁷⁹. Thus, the diminished expression of *ACH1* in *gunSOS1* compared with *sigRep* (Supplementary Fig. 10a,b) and plausible inactivation of *ACH1* by fumarate, together may constitute factors leading to aconitate depletion in *gunSOS1* cells exposed to $^1\text{O}_2$ stress.

Simultaneous increase in the *ACH1* expression and the rescue of the $^1\text{O}_2$ -signalling upon exogenously applied aconitate might be pointing to rather aconitase function than the sole aconitate effect on these processes. In animal cells, aconitase redox-regulated moonlighting function modulates biosynthesis of proteins carrying Iron Response Element (IRE) in their mRNA^{45,80–82}. The dual function of aconitase is possible due to the reversible redox-dependent post-translational modifications (reviewed in⁸¹). Three cysteines crucial for binding the iron-sulphur cluster in mitochondrial ACO2 in mouse, Cys385, Cys448, and Cys451⁷⁹, are also present in *ACH1* of *C. reinhardtii*, Cys426, Cys489, and Cys492, respectively.

Aconitase emerges as a factor involved in stress response also in plants. In *A. thaliana*, aconitase (ACO) is found in three isoforms. ACO3 in *A. thaliana* serves both as a target and mediator of mitochondrial dysfunction signalling, and it was shown to be critical for stress response in leaves⁸³. Phosphorylation of ACO3-Ser91 contributes to the UV-B and mitochondrial complex III inhibitor antimycin A-induced stress tolerance⁸³. *ACH1* of *C. reinhardtii* contains four serine residues within a widely conserved eukaryotic phosphorylation motif R-x-x-S⁸⁴, Ser118, Ser211, Ser284, and Ser439, so their phosphorylation is likely. ACO3 was demonstrated to be part of the mitochondrial dysfunction response, which is dependent on the signalling involving transcription factor NAC domain containing protein 17 (ANAC017). ANAC017 is considered as a master regulator of the retrograde signalling and cellular stress response

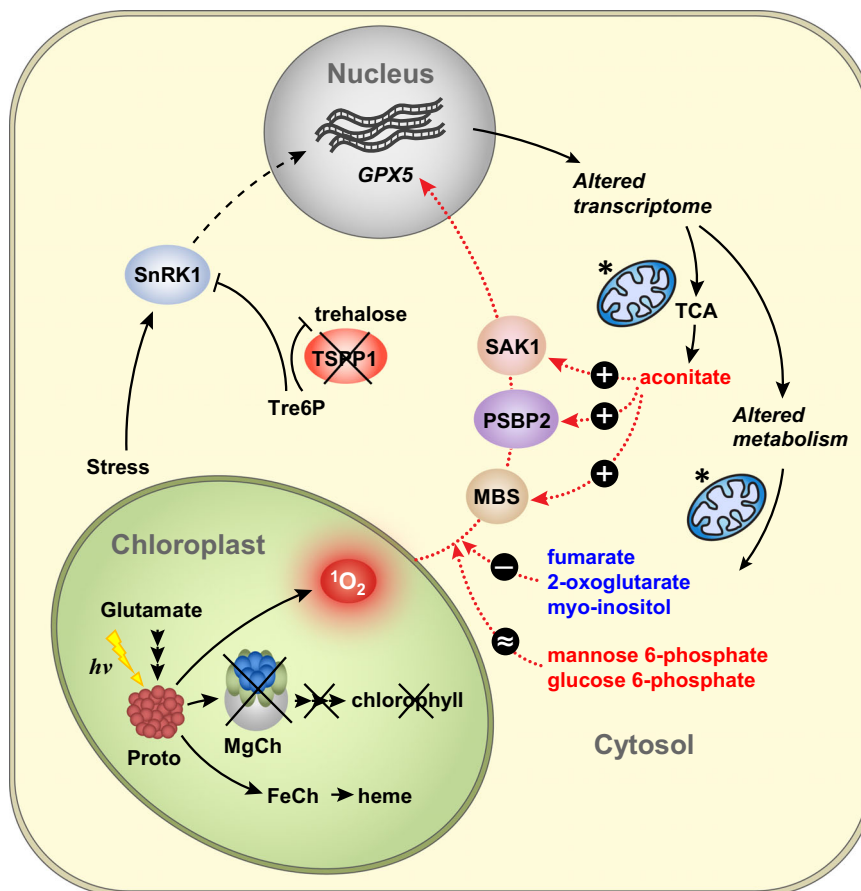


Fig. 7 Model of the chloroplast $^1\text{O}_2$ -induced retrograde signalling depending on the metabolites content. Lack of a functional Mg-chelatase (MgCh) leads to accumulation of protoporphyrin IX (Proto), which in light generates $^1\text{O}_2$. Absence of TSPP1 results in accumulation of trehalose 6-phosphate (Tre6P). In plants, Tre6P has an inhibitory effect on SnRK1^{45,69,70}, while altered SnRK1 activity is also involved in stress responses in *C. reinhardtii*^{75–78}. Blocked SnRK1 signalling pathway leads to the inadequate transcriptomic response to stress and disturbed metabolites content. Selected metabolites with altered content in *gunSOS1* relative to *sigRep* are shown, increased in blue, decreased in red. Exogenous application of fumarate, 2-oxoglutarate, and myo-inositol always had an inhibitory effect on $^1\text{O}_2$ -signalling in *sigRep*, while no change was observed in *gunSOS1* and WT, relative to their respective non-treated controls. Application of mannose 6-phosphate and glucose 6-phosphate at 20 and 50 μM each increased the expression of GPX5 in *sigRep*, but no change in GPX5 mRNA was observed in *gunSOS1*. Exogenous application of aconitate promoted expression of PSBP2, MBS, and SAK1, and consequently also GPX5, which ultimately indicated the rescue of $^1\text{O}_2$ -signalling in *gunSOS1*. Intracellular localisation of TSPP1, SnRK1, and PSBP2 depicted in the Figure has not been determined experimentally and has only an illustrative character. Mitochondria are marked by an asterisk.

with mitochondria acting as central sensors, but also during repression of the chloroplast function⁸⁵. Based on the genome-wide association study concerning single nucleotide polymorphism, it was determined that promoter of ACO3 binds ANAC017⁸⁶.

ACO3 plays an important role in acclimation to submergence⁸⁶ and it was proposed to regulate the stability of chloroplast superoxide dismutase 2 (SOD2) mRNA⁸⁷. Both submergence-related hypoxia and reoxygenation during desubmergence are accompanied by increased ROS generation and oxidative stress^{88,89}. The *aco3* knockout mutant and ACO3 overexpressing lines (ACO3OE) showed altered stress signalling correlated with decreased and increased stress tolerance, respectively. Furthermore, a decreased expression of fumarate 2 (FUM2) was noted in ACO3OE lines in the control conditions, and it decreased in *aco3*, ACO3OE, and in WT after submergence and desubmergence⁸⁶. The JGI portal blast-search analysis of *A. thaliana* FUM2 against *C. reinhardtii* proteome indicated, that the protein showing the highest similarity in amino acid sequence is the FUM2, which showed increased expression in *gunSOS1* compared with *sigRep* (Supplementary Fig. 8c, see also Supplementary Data 2 and 3). These findings provide additional support

for the hypothesis regarding a reciprocal interplay between fumarate and aconitate in response to stress.

Based on our results, including increased expression of ACH1 upon application of aconitate (Fig. 6h), and current knowledge, it can be hypothesized that not aconitate, but ACH1 is the crucial player in $^1\text{O}_2$ -signalling in *C. reinhardtii*, while accumulation of fumarate deactivates ACH1, thereby impairing oxidative stress sensing and $^1\text{O}_2$ -signalling. Chloroplasts and mitochondria are biochemically connected^{90,91}, while the function of the components localised in either compartment has been shown to be integrated into the functional signalling^{92–96}. Therefore, it seems plausible that the mitochondrial function participates, or is even required for functional chloroplast-emitted $^1\text{O}_2$ -signalling. The chloroplast $^1\text{O}_2$ -signal might be providing an input into the overall signalling network, which is subsequently integrated or dependent on the mitochondrial retrograde signalling and other internal or external stimuli.

Our results regarding increased content of fumarate and decreased aconitate in *gunSOS1* compared with *sigRep* (Fig. 3 and Supplementary Figs. 5 and 6) as well as feeding experiments (Fig. 6) indicate, that there is a metabolic signature conditioning $^1\text{O}_2$ -signalling. However, it should be noted that the extent to

which exogenously applied fumarate and aconitate are taken up into the cells was not determined. Nevertheless, treatment with fumarate and aconitate, both have a very clear impact on gene expression (Fig. 6), which would not take place, if these metabolites were not taken up or sensed by the cells. Although, there are no known receptors detecting the presence of these metabolites outside of the cell, their existence cannot be excluded at this point. In either case, it was shown that altered chloroplast redox conditions result in changes in the metabolome in *A. thaliana*, reflected also by the reallocation of energy resources⁹⁷. Importantly, although our study shows that the metabolic configuration of the cell is essential for ¹O₂-signalling, this does not exclude the involvement of protein components in this signalling network (Fig. 7). On the contrary, our findings support the direct involvement of proteins in ¹O₂-signalling, but we demonstrated that expression of *PSBP2*¹⁵, *MBS17*, and *SAK1*¹⁶ depends on the metabolic status (Fig. 5a and Fig. 6g). The overlap between the *gunSOS1* and the *SAK1*-dependent transcriptomes (Fig. 5b) as well as other defined ROS or RES-dependent signalling pathways apparently being functional (Supplementary Fig. 11) indicate specificity of the impaired ¹O₂-signalling in *gunSOS1*. Our results indicate that fumarate and aconitate affect the expression of *PSBP*, *MBS*, or *SAK1* upon ¹O₂-exposure in light, which subsequently convey information about the metabolic status of the cell to the nucleus and trigger specific responses (Fig. 7). It is not clear yet how the specificity of the signalling is achieved, because the mechanisms by which metabolites affect the expression of these proteins, as well as downstream components of these signalling pathways, remain unknown. Additionally, the protein components involved in ¹O₂-signalling may be subject to additional regulatory mechanisms, such as phosphorylation, as proposed for *SAK1* by Wakao et al.¹⁶.

We have shown that retrograde signalling triggered by ¹O₂, which is mostly generated in the chloroplast, strictly depends on the mitochondrial metabolic status. Prolyl-tRNA synthetase (PRORS1) in *A. thaliana*, a component of the organellar gene expression machinery indicated in the previous study that mitochondria may contribute to chloroplast retrograde signalling⁹⁵. PRORS1 is targeted both to the plastid and to mitochondria, but downregulation of specific photosynthesis-associated nuclear genes was observed only in a plastidial *prp11* and mitochondrial *mrp11* double mutant, but not in *prp11* or *mrp11* single mutants⁹⁵. Another study showed that the ROS-dependent signals from chloroplast and mitochondria are integrated at the radical-induced cell death 1 (RCD1) protein located in the nucleus⁹⁶. RCD1 suppresses transcription factors ANAC013 and ANAC017, which mediate the ROS-signal from mitochondria, while chloroplast regulation of RCD1 takes place through 3'-phosphoadenosine 5'-phosphate. It was proposed that RCD1 may function at the intersection of mitochondrial and chloroplastic retrograde signalling pathways⁹⁶.

The retrograde signalling pathways identified so far assume the existence of separate signalling routes. However, chloroplast retrograde signalling involves a network of different but interconnected mechanisms, and observation of specific signalling pathways within the network depends on the experimental conditions. Pharmacological or genetic interventions that disrupt specific pathways can be used to characterise alternative pathways. In the manuscript presented here, we report that the metabolic status of the cell, reflecting levels of Tre6P, and components of the mitochondrial TCA cycle, are integral factors in the ¹O₂-dependent retrograde signalling network in *C. reinhardtii*. It remains a matter of debate whether Tre6P or TSPP1 protein itself plays a direct role in the signalling and metabolic reprogramming. Additionally, further study should elucidate whether aconitate or ACH1 is the key player in the

¹O₂-signalling. Nevertheless, our results shed an important light on the signalling processes triggered by ¹O₂, by revealing their sensitivity to metabolites and thereby their potential modulation by cytosolic and mitochondrial metabolism.

Methods

***Chlamydomonas reinhardtii* cultures and genetic manipulations.** All strains were cultivated heterotrophically in Tris-acetate-phosphate (TAP) medium in the dark until reaching the mid-log phase of 3–5 × 10⁶ cells mL⁻¹. Additionally, starch measurements were performed in TAP, Tris-phosphate (TP) medium without acetate, or nitrogen-depleted (TAP-N) medium. Experiments were performed in TAP medium in the dark or upon a shift to 20 μmol photons m⁻² s⁻¹ light. Sampling of three separate cultures grown in parallel in the same conditions was considered as biological replicates. Three strains used in this study were described elsewhere, *chd1-1* in von Gromoff, et al.¹⁸, *chd1-GUN4* in ref. ¹⁹, and WT (4A+) in ref. ⁹⁸.

To generate the *GPX5-ARS2* construct (Supplementary Fig. 2), the *GPX5* regulatory region (*GPX5* 5' RR) was amplified by PCR using forward and reverse primers carrying XhoI and EcoRV restriction sites, respectively (Supplementary Table 20). The obtained fragment was subcloned and ligated between the XhoI/EcoRV sites of the pSL18 vector⁹⁹, replacing the existing promoter region of the gene encoding the PSAD and positioning *GPX5* 5'RR in reverse orientation with respect to the paromomycin resistance cassette (*paroR*¹⁰⁰). The DNA fragment carrying *paroR* and *GPX5* 5' RR was excised by restriction digestion with KpnI and EcoRV and ligated into the corresponding restriction sites of pJD54¹⁰¹, which carries a copy of the promoterless version of the gene encoding arylsulfatase 2 (*ARS2*), which allowed *ARS2* expression to be controlled by the *GPX5* 5'RR (Supplementary Fig. 2). The *GPX5-ARS2* construct was verified by sequencing.

The *sigRep* strain was produced in the *chd1-GUN4* background by transformation with a *GPX5-ARS2* construct. Transformant selection was performed on TAP agar plates with 10 μg mL⁻¹ paromomycin in the dark, followed by a screen for *GPX5-ARS2* inducibility by ¹O₂. The *sigRep* strain showed low *ARS2* activity in the dark and high activity in the light (Fig. 1a) and was selected for further applications. The *gunSOS1* mutant was generated by random insertional mutagenesis performed on *sigRep* using a bleomycin resistance cassette (*ble*^R) isolated from the pMS188 vector¹⁰² using NotI and KpnI. Following mutagenesis, selection was performed on TAP agar plates containing 15 μg mL⁻¹ zeocin in the dark. More than 800 obtained colonies were screened for decreased or not detectable *ARS2* activity in the light and nine mutants that showed impaired inducibility of *GPX5-ARS* expression in light were selected for further analysis. Restriction enzyme site-directed amplification PCR¹⁰³ allowed us to identify the genomic DNA flanking the *ble*^R insertion sites in five out of the nine mutants. Only analysis of the *gunSOS1* mutant is presented here. Rescue of *gunSOS1* (*tssp1*) was conducted with 5242 bp fragment of genomic DNA carrying 3241 bp *TSPP1* amplified by PCR (see Supplementary Table 20 for primers) using bacterial artificial chromosome PTQ5987 (Clemson University Genomics Institute, Clemson, SC, USA) as a template. The amplified DNA fragment included 1500 bp upstream and 501 bp downstream of the annotated *TSPP1*. WT *TSPP1* was introduced into *gunSOS1* by co-transformation with a spectinomycin resistance cassette isolated from the pALM32 vector¹⁰⁴ with AelI and KpnI endonucleases. Transformant selection was performed on TAP agar plates supplemented with 100 μg mL⁻¹ spectinomycin in the dark. All genetic transformations were performed by electroporation.

Arylsulfatase activity assay. To assess the level of *GPX5-ARS2* expression in transformed cells, enzymatic assays for arylsulfatase activity²⁵ were performed essentially as described before ref. ¹⁵. Cells were spotted onto agar-solidified TAP medium plates and cultured in either light or dark conditions. Arylsulfatase is expected to be secreted into the medium if *GPX5-ARS2* is expressed. After removal of the cells, plates were flooded with detection solution containing 0.1 mg mL⁻¹ 2-naphthyl sulphate (potassium salt; Santa Cruz Biotechnology, Inc., Dallas, TX, USA) as a chromogenic substrate coupled with 1 mg mL⁻¹ tetrazotized-o-dianisidine chloride (Fast Blue B salt, Santa Cruz Biotechnology, Inc., Dallas, TX, USA). Following 1 h incubation, purple spots appearing on the agar plates identified expressed *ARS2*.

Analysis of protoporphyrin IX content. The Proto content was analysed by High Pressure Liquid Chromatography (HPLC) essentially as described in ref. ¹⁰⁵, with modified sample preparation for *C. reinhardtii*¹⁹. In short, cultures were grown in the dark and transferred to 20 μmol photons m⁻² s⁻¹ light for 2 h. Samples containing 1.2 × 10⁸ cells were centrifuged at 3000 × g for 5 min at 4 °C and the pellets were snap-frozen in liquid N₂. Proto was extracted in cold (-20 °C) acetone/0.1 M NH₄OH (9/1, v/v) in a three-step cycle of resuspension and centrifugation. Proto analysis was performed using a Nova-Pak C18 column (Waters, 3.9 × 150 mm, 4 μm, at 20 °C). The results were normalised to pmol/10⁶ cells.

RNA isolation, qRT-PCR, and RNA-seq. The total RNA was isolated, after a shift from dark to 20 μmol photons m⁻² s⁻¹ light for 2 h, using TRIzol Reagent

(Thermo Fisher Scientific, Waltham, MA, USA), according to the manufacturer's protocol. RNA quality was assessed by electrophoresis on a 1% (w/v) agarose gel, while quantity was determined using a Nanodrop 2000 (Thermo Fischer Scientific, Waltham, MA). Aliquots of 2 µg RNA were treated with DNase and RiboLock RNase inhibitor (Thermo Fisher Scientific, Waltham, MA, USA) and used to synthesise cDNA with RevertAid Reverse Transcriptase (Thermo Fisher Scientific, Waltham, MA, USA) and oligo(dT)₁₈ primer. Transcript analysis by qRT-PCR were performed using 2× ChamQ Universal SYBR qPCR Master Mix (Viazyme Biotech Co., Ltd., Nanjing, China) and a CFX96-C1000 96-well plate thermocycler (Bio-Rad, Hercules, CA, USA). In the initial experiments, determining expression kinetics of *GPX5* (Fig. 1b) and *GPX5-ARS2* (Fig. 1c), we observed change in the 18 S rRNA quantification cycle (Cq) by ≤ 3.3 in dark compared with subsequent exposure to 2 h light (Supplementary Table 21), both in *sigRep* and WT. Nevertheless, the difference in averaged 18 S Cq between *sigRep* and WT from the same conditions was always ≤ 0.9 , which indicated sufficient consistency in 18 S expression regardless of the cell line and photooxidative stress. These results indicated suitability of 18 S to be used as a reference gene for qRT-PCR experiments. Most primers for transcript analyses were designed using Primer3Plus (<http://primer3plus.com>). Wherever applicable, the same primers were used as in the previous gene expression studies. All primers and their references are listed in Supplementary Table 20.

RNA-sequencing was performed on total RNA samples isolated from biological triplicates of *sigRep* and *gunSOS1* after the shift from dark to 20 µmol photons m⁻² s⁻¹ light for 2 h. Library preparation, sequencing, and analysis services were commercially provided by Novogene Europe (Novogene (UK) Company Ltd., Cambridge, UK) and performed using an Illumina NovaSeq 6000 platform operated in 150 bp pair-end sequencing mode, with a sequencing depth of 20 million reads per sample. Six gigabases of sequencing data per library was filtered for high-quality reads, which were mapped to the *C. reinhardtii* v5.5 (Department of Energy JGI). Estimated expression was obtained in fragments per kilobase of transcript sequence per millions base pairs sequenced (FPKM). Biological replicates were averaged to obtain sample expression estimate. Differential expression analysis between two mutants (three biological replicates per mutant) was performed using DESeq2.v1.20.0, which provides statistical routines for determining differential expression using a model based on the negative binomial distribution. The resulting *p* values were adjusted using the Benjamini and Hochberg's approach for controlling the False Discovery Rate (FDR). Genes with a log₂FoldChange ≥ 2 and adjusted *p* value (padj) < 0.05 found by DESeq2.v1.20.0 were defined as differentially expressed (DEGs). Gene Ontology (GO) analysis and Kyoto Encyclopedia of Genes and Genomes (KEGG; www.genome.jp/kegg/pathway.html) pathway analysis were conducted to identify DEGs at the biologically functional level using clusterProfiler R package. GO terms and KEGG pathways with a padj < 0.05 were considered to be significantly enriched.

Metabolite analysis. Cultures were grown in TAP in the dark until they reached mid-log phase of 3×10^6 cells mL⁻¹. Samples were always normalised to contain 6×10^7 cells, all centrifugation steps were carried at $3000 \times g$ at 4 °C for 5 min, followed by snap-freezing in liquid N₂. Samples from dark conditions were collected immediately, while the remainder of each culture was transferred to 20 µmol photons m⁻² s⁻¹ light. Subsequent sampling took place at 15-min intervals, up to 1 h. Metabolites were extracted using chloroform-methanol as described by Lunn et al.²⁸. Tre6P, other phosphorylated intermediates and organic acids were measured by anion-exchange HPLC coupled to tandem mass spectrometry (LC-MS/MS) as described in ref.²⁸ with modifications as described in ref.¹⁰⁶. Sugars and sugar alcohols were measured by LC-MS/MS as described in ref.¹⁰⁷. Obtained results were normalised to pmol/10⁶ cells.

For starch analysis, cultures were grown in TAP in the dark until they reached mid-log phase of 3×10^6 cells mL⁻¹. For starch determination cultures were either transferred in TAP to the light (20 µmol photons m⁻² s⁻¹) for 2 h before harvesting, or centrifuged cells were resuspended in Tris-phosphate (TP) medium (without acetate), keeping the same cell concentration, and transferred back to the dark for 24 h. Subsequently, cultures were transferred to 20 µmol photons m⁻² s⁻¹ for 2 h before harvesting. A similar protocol was applied for starch analysis in TAP devoid of N (TAP-N), except that cells were cultivated in TAP-N for 3 days in the dark, followed by exposure to 20 µmol photons m⁻² s⁻¹ for 2 h. For each sampling, 5×10^6 cells were centrifuged and lyophilized. Starch content was determined by enzymatic degradation and glucose quantification following the protocol of ref.¹⁰⁸.

Protein extraction and immunoblot analysis. Cultures were grown in the dark until reaching the mid-log phase of $3\text{--}5 \times 10^6$ cells mL⁻¹, followed by a transfer to 20 µmol photons m⁻² s⁻¹ for 3 h. Cells were pelleted by centrifugation and total proteins were extracted in 400 µL buffer containing: 56 mM Na₂CO₃, 56 mM DTT, 2% (w/v) SDS, 12% (w/v) sucrose and 2 mM EDTA, pH 8.0. Proteins were quantified using Pierce™ BCA Protein Assay Kit (Thermo Fisher Scientific, Waltham, MA, USA) and separated by SDS-PAGE on a 12% polyacrylamide gel, followed by transfer by electroblotting to nitrocellulose membrane (GE Healthcare, Chicago, IL, USA). TSPP1 was detected using a rabbit crude antiserum (dilution 1:500) raised by inoculation with a TSPP1-specific peptide (VEWSKSDSNG-WRAKPC) against *C. reinhardtii* TSPP1 (calculated MW 42 kDa). GPX5 was detected with a commercially available antibody (AS15 2882, dilution 1:1000) obtained from Agrisera (Vännäs, Sweden). CHLI1 antibody (PHY5510S, dilution

1:1000) was purchased from PhytoAB (San Jose, CA, USA). For application, all antibodies were diluted in CrossDown buffer (AppliChem, AppliChem GmbH, Darmstadt, Germany). The secondary antibody (AS09 602, goat anti-rabbit IgG, dilution 1:10,000) conjugated to horseradish peroxidase was obtained from Agrisera. The immunoblotting signals were detected using a CCD camera (Intas Biopharmaceuticals, Ahmedabad, India) after application of enhanced chemiluminescence detection kit (Clarity™ Western ECL Substrate; Bio-Rad, Hercules, CA, USA).

Chemical treatments of *C. reinhardtii* cells. Fumarate (sodium fumarate dibasic), 2-oxoglutarate (α-ketoglutaric acid), myo-inositol (D-myo-inositol 1,4,5-trisphosphate trisodium salt), mannose 6-phosphate (D-mannose-6-phosphate, disodium salt), glucose 6-phosphate (D-glucose 6-phosphate sodium salt), and acornitate (*cis*-aconitic acid) were obtained from Sigma-Aldrich (Sigma-Aldrich Chemie GmbH, Taufkirchen, Germany), dissolved in H₂O to a stock solutions of 100 mM and added individually to the mid-log phase (3×10^6 cells mL⁻¹) cultures to final concentrations of 20, 50, and 100 µM, followed by exposure to light for 2 h.

Statistics and reproducibility. Statistical analyses were conducted using the GraphPad Prism 9 for Windows, version 9.5.0 (GraphPad Software, San Diego, California USA, www.graphpad.com). All the details concerning particular analysis are included in the main text, in the Figure legend, or in the Supplementary Table, wherever applicable.

Reporting summary. Further information on research design is available in the Nature Portfolio Reporting Summary linked to this article.

Data availability

All data relevant for interpretation of this study are presented in the article and supplementary material, including uncropped and unedited blot images for Fig. 2d (Supplementary Fig. 12). The numerical source data for all the graphs presented in the main Figures are provided in Supplementary Data 4. The raw RNA-seq data were deposited in the National Center for Biotechnology Information Sequence Read Archive, accession number [PRJNA954977](https://www.ncbi.nlm.nih.gov/submit/PRJNA954977). Any further information is available from the corresponding author upon reasonable request.

Received: 15 June 2022; Accepted: 24 April 2023;

Published online: 16 May 2023

References

- Johanningmeier, U. & Howell, S. H. Regulation of light-harvesting chlorophyll-binding protein mRNA accumulation in *Chlamydomonas reinhardtii*. Possible involvement of chlorophyll synthesis precursors. *J. Biol. Chem.* **259**, 3541–3549 (1984).
- Oelmüller, R. Photooxidative destruction of chloroplasts and its effect on nuclear gene expression and extraplastidic enzyme levels. *Photochem. Photobiol.* **49**, 229–239 (1989).
- Susek, R. E., Ausubel, F. M. & Chory, J. Signal transduction mutants of Arabidopsis uncouple nuclear CAB and RBCS gene expression from chloroplast development. *Cell* **74**, 787–799 (1993).
- Oster, U., Brunner, H. & Rudiger, W. The greening process in cress seedlings .5. Possible interference of chlorophyll precursors, accumulated after thujaplicin treatment, with light-regulated expression of Lhc genes. *J. Photoch. Photobiol. B* **36**, 255–261 (1996).
- Lydon, J. & Duke, S. O. Porphyrin synthesis is required for photobleaching activity of the para-nitrosubstituted diphenyl ether herbicides. *Pestic. Biochem. Physiol.* **31**, 74–83 (1988).
- Triantaphylides, C. et al. Singlet oxygen is the major reactive oxygen species involved in photooxidative damage to plants. *Plant Physiol.* **148**, 960–968 (2008).
- op den Camp, R. G. L. et al. Rapid induction of distinct stress responses after the release of singlet oxygen in Arabidopsis. *Plant Cell* **15**, 2320–2332 (2003).
- Gorman, A. A. & Rodgers, M. A. J. Current perspectives of singlet oxygen detection in biological environments. *J. Photoch. Photobiol. B* **14**, 159–176 (1992).
- Beck, C. F. Signaling pathways from the chloroplast to the nucleus. *Planta* **222**, 743–756 (2005).
- Sies, H. & Menck, C. F. M. Singlet oxygen induced DNA damage. *Mutat. Res.* **275**, 367–375 (1992).
- Björn, L. O. *Photobiology: The Science of Life and Light*, Springer. (2008).
- Pfannschmidt, T. Plastidial retrograde signalling - a true "plastid factor" or just metabolite signatures? *Trends Plant Sci.* **15**, 427–435 (2010).

13. Kleine, T., Voigt, C. & Leister, D. Plastid signalling to the nucleus: messengers still lost in the mists? *Trends Genet.* **25**, 185–190 (2009).
14. Kim, C. et al. Chloroplasts of Arabidopsis are the source and a primary target of a plant-specific programmed cell death signaling pathway. *Plant Cell* **24**, 3026–3039 (2012).
15. Brzezowski, P., Wilson, K. E. & Gray, G. R. The PSBP2 protein of *Chlamydomonas reinhardtii* is required for singlet oxygen-dependent signaling. *Planta* **236**, 1289–1303 (2012).
16. Wakao, S. et al. Phosphoprotein SAK1 is a regulator of acclimation to singlet oxygen in *Chlamydomonas reinhardtii*. *eLife* **3**, e02286 (2014).
17. Shao, N., Duan, G. Y. & Bock, R. A mediator of singlet oxygen responses in *Chlamydomonas reinhardtii* and Arabidopsis identified by a luciferase-based genetic screen in algal cells. *Plant Cell* **25**, 4209–4226 (2013).
18. von Gromoff, E. D., Alawady, A., Meinecke, L., Grimm, B. & Beck, C. F. Heme, a plastid-derived regulator of nuclear gene expression in *Chlamydomonas*. *Plant Cell* **20**, 552–567 (2008).
19. Brzezowski, P. et al. The GUN4 protein plays a regulatory role in tetrapyrrole biosynthesis and chloroplast-to-nucleus signalling in *Chlamydomonas reinhardtii*. *Plant J.* **79**, 285–298 (2014).
20. Fischer, B. B., Krieger-Liszka, A. & Eggen, R. I. L. Photosensitizers neutral red (Type I) and rose bengal (Type II) cause light-dependent toxicity in *Chlamydomonas reinhardtii* and induce the Gpxh gene via increased singlet oxygen formation. *Environ. Sci. Technol.* **38**, 6307–6313 (2004).
21. Ledford, H. K., Chin, B. L. & Niyogi, K. K. Acclimation to singlet oxygen stress in *Chlamydomonas reinhardtii*. *Eukaryot. Cell* **6**, 919–930 (2007).
22. Meskauskiene, R. et al. FLU: A negative regulator of chlorophyll biosynthesis in *Arabidopsis thaliana*. *Proc. Natl. Acad. Sci. USA* **98**, 12826–12831 (2001).
23. Hou, Z., Yang, Y., Hedtke, B. & Grimm, B. Fluorescence in blue light (FLU) is involved in inactivation and localization of glutamyl-tRNA reductase during light exposure. *Plant J.* **97**, 517–529 (2019).
24. Leisinger, U. et al. The glutathione peroxidase homologous gene from *Chlamydomonas reinhardtii* is transcriptionally up-regulated by singlet oxygen. *Plant Mol. Biol.* **46**, 395–408 (2001).
25. Ohresser, M., Matagne, R. F. & Loppes, R. Expression of the arylsulphatase reporter gene under the control of the nit1 promoter in *Chlamydomonas reinhardtii*. *Curr. Genet.* **31**, 264–271 (1997).
26. Fischer, B. B., Il Eggen, R. & Niyogi, K. K. Characterization of singlet oxygen-accumulating mutants isolated in a screen for altered oxidative stress response in *Chlamydomonas reinhardtii*. *BMC Plant Biol.* **10**, 279 (2010).
27. Fischer, B. B. et al. Function and regulation of the glutathione peroxidase homologous gene GPXH/GPX5 in *Chlamydomonas reinhardtii*. *Plant Mol. Biol.* **71**, 569–583 (2009).
28. Lunn, J. E. et al. Sugar-induced increases in trehalose 6-phosphate are correlated with redox activation of ADPglucose pyrophosphorylase and higher rates of starch synthesis in *Arabidopsis thaliana*. *Biochem. J.* **397**, 139–148 (2006).
29. Yadav, U. P. et al. The sucrose-trehalose 6-phosphate (Tre6P) nexus: specificity and mechanisms of sucrose signalling by Tre6P. *J. Exp. Bot.* **65**, 1051–1068 (2014).
30. Schluempmann, H., Pellny, T., van Dijken, A., Smeekens, S. & Paul, M. Trehalose 6-phosphate is indispensable for carbohydrate utilization and growth in *Arabidopsis thaliana*. *Proc Natl Acad Sci USA* **100**, 6849–6854 (2003).
31. Fichtner, F. & Lunn, J. E. The role of trehalose 6-phosphate (Tre6P) in plant metabolism and Development. *Annu. Rev. Plant Biol.* **72**, 737–760 (2021).
32. Miller, R. et al. Changes in transcript abundance in *Chlamydomonas reinhardtii* following nitrogen deprivation predict diversion of metabolism. *Plant Physiol.* **154**, 1737–1752 (2010).
33. Ajalla Aleixo, M. A., Rangel, V. L., Rustiguel, J. K., de Pádua, R. A. P. & Nonato, M. C. Structural, biochemical and biophysical characterization of recombinant human fumarate hydratase. *FEBS J.* **286**, 1925–1940 (2019).
34. Yogeve, O. et al. Fumarase: a mitochondrial metabolic enzyme and a cytosolic/nuclear component of the DNA damage response. *PLoS Biol.* **8**, e1000328 (2010).
35. Jiang, Y. et al. Local generation of fumarate promotes DNA repair through inhibition of histone H3 demethylation. *Nat. Cell Biol.* **17**, 1158–1168 (2015).
36. Ma, X. et al. Transcriptomic and physiological responses to oxidative stress in a *Chlamydomonas reinhardtii* glutathione peroxidase mutant. *Genes* **11**, <https://doi.org/10.3390/genes11040463> (2020).
37. Yang, M., Soga, T., Pollard, P. J. & Adam, J. The emerging role of fumarate as an oncometabolite. *Frontiers in oncology* **2**, 85 (2012).
38. Ferrario-Méry, S. et al. Glutamine and alpha-ketoglutarate are metabolite signals involved in nitrate reductase gene transcription in untransformed and transformed tobacco plants deficient in ferredoxin-glutamine-alpha-ketoglutarate aminotransferase. *Planta* **213**, 265–271 (2001).
39. Lancien, M., Gadal, P. & Hodges, M. Enzyme redundancy and the importance of 2-oxoglutarate in higher plant ammonium assimilation. *Plant Physiol.* **123**, 817–824 (2000).
40. Feria Bourrellier, A. B., Ferrario-Méry, S., Vidal, J. & Hodges, M. Metabolite regulation of the interaction between Arabidopsis thaliana PII and N-acetyl-L-glutamate kinase. *Biochem. Biophys. Res. Commun.* **387**, 700–704 (2009).
41. Gillaspay, G. E. The cellular language of myo-inositol signaling. *New Phytol.* **192**, 823–839 (2011).
42. Toroser, D., Plaut, Z. & Huber, S. C. Regulation of a plant SNF1-related protein kinase by glucose-6-phosphate. *Plant Physiol.* **123**, 403–412 (2000).
43. Zhang, Y. et al. Inhibition of SNF1-related protein kinase1 activity and regulation of metabolic pathways by trehalose-6-phosphate. *Plant Physiol.* **149**, 1860–1871 (2009).
44. Flint, D. H., Tuminello, J. F. & Emptage, M. H. The inactivation of Fe-S cluster containing hydro-lyases by superoxide. *J. Biol. Chem.* **268**, 22369–22376 (1993).
45. Bulteau, A. L., Ikeda-Saito, M. & Szewda, L. I. Redox-dependent modulation of aconitase activity in intact mitochondria. *Biochemistry* **42**, 14846–14855 (2003).
46. Blaby, I. K. et al. Genome-wide analysis on *Chlamydomonas reinhardtii* reveals the impact of hydrogen peroxide on protein stress responses and overlap with other stress transcripts. *Plant J.* **84**, 974–988 (2015).
47. Urzica, E. I. et al. Impact of oxidative stress on ascorbate biosynthesis in *Chlamydomonas* via regulation of the VTC2 gene encoding a GDP-L-galactose phosphorylase. *J. Biol. Chem.* **287**, 14234–14245 (2012).
48. Roach, T., Stögl, W., Baur, T. & Kranter, I. Distress and eustress of reactive electrophiles and relevance to light stress acclimation via stimulation of thiol/disulphide-based redox defences. *Free Rad. Biol. Med.* **122**, 65–73 (2018).
49. Arora, A., Sairam, R. K. & Srivastava, G. C. Oxidative stress and antioxidative system in plants. *Curr. Sci.* **82**, 1227–1238 (2002).
50. Moller, I. M. Plant mitochondria and oxidative stress: Electron transport, NADPH turnover, and metabolism of reactive oxygen species. *Annu. Rev. Plant Physiol. Plant Mol. Biol.* **52**, 561–591 (2001).
51. Asada, K. Production and scavenging of reactive oxygen species in chloroplasts and their functions. *Plant Physiol.* **141**, 391–396 (2006).
52. Brzezowski, P., Richter, A. S. & Grimm, B. Regulation and function of tetrapyrrole biosynthesis in plants and algae. *Biochimica Et Biophysica Acta-Bioenergetics* **1847**, 968–985 (2015).
53. Larkin, R. M. Tetrapyrrole signaling in plants. *Front. Plant Sci.* **7**, <https://doi.org/10.3389/fpls.2016.01586> (2016).
54. Moulin, M., McCormac, A. C., Terry, M. J. & Smith, A. G. Tetrapyrrole profiling in Arabidopsis seedlings reveals that retrograde plastid nuclear signaling is not due to Mg-protoporphyrin IX accumulation. *Proc. Natl. Acad. Sci. USA* **105**, 15178–15183 (2008).
55. Mochizuki, N., Tanaka, R., Tanaka, A., Masuda, T. & Nagatani, A. The steady-state level of Mg-protoporphyrin IX is not a determinant of plastid-to-nucleus signaling in Arabidopsis. *Proc. Natl. Acad. Sci. USA* **105**, 15184–15189 (2008).
56. Vandesteene, L. et al. Expansive evolution of the trehalose-6-phosphate phosphatase gene family in Arabidopsis. *Plant Physiol.* **160**, 884–896 (2012).
57. Ramon, M. et al. Extensive expression regulation and lack of heterologous enzymatic activity of the Class II trehalose metabolism proteins from Arabidopsis thaliana. *Plant Cell Environ.* **32**, 1015–1032 (2009).
58. Vandesteene, L., Ramon, M., Le Roy, K., Van Dijk, P. & Rolland, F. A single active trehalose-6-P synthase (TPS) and a family of putative regulatory TPS-like proteins in Arabidopsis. *Mol. Plant* **3**, 406–419 (2010).
59. Delorge, I., Figueroa, C. M., Feil, R., Lunn, J. E. & Van Dijk, P. Trehalose-6-phosphate synthase 1 is not the only active TPS in Arabidopsis thaliana. *Biochem. J.* **466**, 283–290 (2015).
60. Collet, J. F., Stroobant, V., Pirard, M., Delpierre, G. & Van Schaftingen, E. A new class of phosphotransferases phosphorylated on an aspartate residue in an amino-terminal DXDX(T/V) motif. *J. Biol. Chem.* **273**, 14107–14112 (1998).
61. Martins, M. C. et al. Feedback inhibition of starch degradation in Arabidopsis leaves mediated by trehalose 6-phosphate. *Plant Physiol.* **163**, 1142–1163 (2013).
62. Dos Anjos, L. et al. Feedback regulation by trehalose 6-phosphate slows down starch mobilization below the rate that would exhaust starch reserves at dawn in Arabidopsis leaves. *Plant direct* **2**, e00078 (2018).
63. Satoh-Nagasawa, N., Nagasawa, N., Malcomber, S., Sakai, H. & Jackson, D. A trehalose metabolic enzyme controls inflorescence architecture in maize. *Nature* **441**, 227–230 (2006).
64. Claeys, H. et al. Control of meristem determinacy by trehalose 6-phosphate phosphatases is uncoupled from enzymatic activity. *Nature plants* **5**, 352–357 (2019).
65. Klein, H. et al. Recruitment of an ancient branching program to suppress carpel development in maize flowers. *Proc Natl Acad Sci USA* **119**, <https://doi.org/10.1073/pnas.2115871119> (2022).
66. Kretzschmar, T. et al. A trehalose-6-phosphate phosphatase enhances anaerobic germination tolerance in rice. *Nature plants* **1**, 15124 (2015).
67. Debast, S. et al. Altering trehalose-6-phosphate content in transgenic potato tubers affects tuber growth and alters responsiveness to hormones during sprouting. *Plant Physiol.* **156**, 1754–1771 (2011).

68. Nunes, C. et al. Inhibition of SnRK1 by metabolites: tissue-dependent effects and cooperative inhibition by glucose 1-phosphate in combination with trehalose 6-phosphate. *Plant Physiol. Biochem.* **63**, 89–98 (2013).
69. Zhai, Z. et al. Trehalose 6-Phosphate Positively Regulates Fatty Acid Synthesis by Stabilizing WRINKLED1. *Plant Cell* **30**, 2616–2627 (2018).
70. Baena-González, E. & Lunn, J. E. SnRK1 and trehalose 6-phosphate - two ancient pathways converge to regulate plant metabolism and growth. *Curr. Opin. Plant Biol.* **55**, 52–59 (2020).
71. Depaepe, T. et al. At the crossroads of survival and death: The reactive oxygen species-ethylene-sugar triad and the unfolded protein response. *Trends Plant Sci.* **26**, 338–351 (2021).
72. Baena-González, E., Rolland, F., Thevelein, J. M. & Sheen, J. A central integrator of transcription networks in plant stress and energy signalling. *Nature* **448**, 938–942 (2007).
73. Gonzalez-Ballester, D., Pollock, S. V., Pootakham, W. & Grossman, A. R. The central role of a SNRK2 kinase in sulfur deprivation responses. *Plant Physiol.* **147**, 216–227 (2008).
74. González-Ballester, D. et al. RNA-seq analysis of sulfur-deprived *Chlamydomonas* cells reveals aspects of acclimation critical for cell survival. *Plant Cell* **22**, 2058–2084 (2010).
75. Colina, F. et al. Genome-wide identification and characterization of CKIN/SnRK gene family in *Chlamydomonas reinhardtii*. *Sci. Rep.* **9**, 350 (2019).
76. Valledor, L., Furuhashi, T., Hanak, A. M. & Weckwerth, W. Systemic cold stress adaptation of *Chlamydomonas reinhardtii*. *Mol. Cell. Proteomics* **12**, 2032–2047 (2013).
77. O’Flaherty, L. et al. Dysregulation of hypoxia pathways in fumarate hydratase-deficient cells is independent of defective mitochondrial metabolism. *Hum. Mol. Genet.* **19**, 3844–3851 (2010).
78. Shanmugasundaram, K. et al. The oncometabolite fumarate promotes pseudohypoxia through noncanonical activation of NF- κ B signaling. *J. Biol. Chem.* **289**, 24691–24699 (2014).
79. Ternette, N. et al. Inhibition of mitochondrial aconitase by succination in fumarate hydratase deficiency. *Cell reports* **3**, 689–700 (2013).
80. Lushchak, O. V., Piroddi, M., Galli, F. & Lushchak, V. I. Aconitase post-translational modification as a key in linkage between Krebs cycle, iron homeostasis, redox signaling, and metabolism of reactive oxygen species. *Redox Rep* **19**, 8–15 (2014).
81. Cairo, G., Recalcati, S., Pietrangelo, A. & Minotti, G. The iron regulatory proteins: targets and modulators of free radical reactions and oxidative damage. *Free radical biology & medicine* **32**, 1237–1243 (2002).
82. Castro, L., Tórtora, V., Mansilla, S. & Radi, R. Aconitases: Non-redox iron-sulfur proteins sensitive to reactive species. *Accounts of chemical research* **52**, 2609–2619 (2019).
83. Pascual, J. et al. ACONITASE 3 is part of the ANAC017 transcription factor-dependent mitochondrial dysfunction response. *Plant Physiol.* **186**, 1859–1877 (2021).
84. Bradley, D. & Belrao, P. Evolution of protein kinase substrate recognition at the active site. *PLoS Biol.* **17**, e3000341 (2019).
85. Meng, X. et al. ANAC017 coordinates organellar functions and stress responses by reprogramming retrograde signaling. *Plant Physiol.* **180**, 634–653 (2019).
86. Meng, X. et al. GWAS on multiple traits identifies mitochondrial ACONITASE3 as important for acclimation to submergence stress. *Plant Physiol.* <https://doi.org/10.1093/plphys/kiac011> (2022).
87. Moeder, W., Del Pozo, O., Navarre, D. A., Martin, G. B. & Klessig, D. F. Aconitase plays a role in regulating resistance to oxidative stress and cell death in *Arabidopsis* and *Nicotiana benthamiana*. *Plant Mol. Biol.* **63**, 273–287 (2007).
88. Pucciariello, C., Parlanti, S., Banti, V., Novi, G. & Perata, P. Reactive oxygen species-driven transcription in *Arabidopsis* under oxygen deprivation. *Plant Physiol.* **159**, 184–196 (2012).
89. Yeung, E., Bailey-Serres, J. & Sasidharan, R. After the Deluge: Plant revival post-flooding. *Trends Plant Sci.* **24**, 443–454 (2019).
90. Raghavendra, A. S. & Padmasree, K. Beneficial interactions of mitochondrial metabolism with photosynthetic carbon assimilation. *Trends Plant Sci.* **8**, 546–553 (2003).
91. Noguchi, K. & Yoshida, K. Interaction between photosynthesis and respiration in illuminated leaves. *Mitochondrion* **8**, 87–99 (2008).
92. Leister, D. Genomics-based dissection of the cross-talk of chloroplasts with the nucleus and mitochondria in *Arabidopsis*. *Gene* **354**, 110–116 (2005).
93. Pesaresi, P., Schneider, A., Kleine, T. & Leister, D. Interorganellar communication. *Curr. Opin. Plant Biol.* **10**, 600–606 (2007).
94. Woodson, J. D. & Chory, J. Coordination of gene expression between organellar and nuclear genomes. *Nature Reviews Genetics* **9**, 383–395 (2008).
95. Pesaresi, P. et al. Nuclear photosynthetic gene expression is synergistically modulated by rates of protein synthesis in chloroplasts and mitochondria. *Plant Cell* **18**, 970–991 (2006).
96. Shapiguzov, A. et al. *Arabidopsis* RCD1 coordinates chloroplast and mitochondrial functions through interaction with ANAC transcription factors. *eLife* **8**, <https://doi.org/10.7554/eLife.43284> (2019).
97. Bräutigam, K. et al. Dynamic plastid redox signals integrate gene expression and metabolism to induce distinct metabolic states in photosynthetic acclimation in *Arabidopsis*. *Plant Cell* **21**, 2715–2732 (2009).
98. Dent, R. M., Haglund, C. M., Chin, B. L., Kobayashi, M. C. & Niyogi, K. K. Functional genomics of eukaryotic photosynthesis using insertional mutagenesis of *Chlamydomonas reinhardtii*. *Plant Physiol.* **137**, 545–556 (2005).
99. Depege, N., Bellafiore, S. & Rochaix, J. D. Role of chloroplast protein kinase Stt7 in LHClI phosphorylation and state transition in *Chlamydomonas*. *Science* **299**, 1572–1575 (2003).
100. Sizova, I., Fuhrmann, M. & Hegemann, P. A *Streptomyces rimosus* aphVIII gene coding for a new type phosphotransferase provides stable antibiotic resistance to *Chlamydomonas reinhardtii*. *Gene* **277**, 221–229 (2001).
101. Davies, J. P., Weeks, D. P. & Grossman, A. R. Expression of the arylsulfatase gene from the β 2-tubulin promoter in *Chlamydomonas reinhardtii*. *Nucleic Acids Res.* **20**, 2959–2965 (1992).
102. Schroda, M., Beck, C. F. & Vallon, O. Sequence elements within an HSP70 promoter counteract transcriptional transgene silencing in *Chlamydomonas*. *Plant J.* **31**, 445–455 (2002).
103. Gonzalez-Ballester, D., de Montaigu, A., Galvan, A. & Fernandez, E. Restriction enzyme site-directed amplification PCR: A tool to identify regions flanking a marker DNA. *Anal. Biochem.* **340**, 330–335 (2005).
104. Meslet-Cladière, L. & Vallon, O. Novel shuttle markers for nuclear transformation of the green alga *Chlamydomonas reinhardtii*. *Eukaryot. Cell* **10**, 1670–1678 (2011).
105. Czarnecki, O., Peter, E. & Grimm, B. in *Chloroplast research in Arabidopsis: Methods and Protocols, Vol II* Vol. 775, 357–385 (2011).
106. Figueroa, C. M. et al. Trehalose 6-phosphate coordinates organic and amino acid metabolism with carbon availability. *Plant J.* **85**, 410–423 (2016).
107. Fichtner, F. et al. Trehalose 6-phosphate is involved in triggering axillary bud outgrowth in garden pea (*Pisum sativum* L.). *Plant J.* **92**, 611–623 (2017).
108. DuBois, M., Gilles, K. A., Hamilton, J. K., Rebers, P. A. & Smith, F. Colorimetric method for determination of sugars and related substances. *Analytical chemistry* **28**, 350–356 (1956).

Acknowledgements

This work was supported by the Deutsche Forschungsgemeinschaft (DFG-GR 936/20-2 to B.G. and P.B.), by the Agence Nationale de la Recherche (ChloroPaths: ANR-14-CE05-0041-01 to X.J.), and by the Max Planck Society (R.F. and J.E.L.). We acknowledge support by the Open Access Publication Fund of Humboldt-Universität zu Berlin.

Author contributions

P.B. designed the research. P.B. and W.A.Y. performed most of the experiments. R.F. and J.E.L. performed the LC-MS/MS measurements. M.S.-S. and X.J. performed the starch quantification. P.B., B.G., and J.E.L. analysed the data. P.B. wrote the manuscript. P.B., B.G., J.E.L., and X.J. revised the manuscript. All authors discussed the results and commented upon the manuscript.

Funding

Open Access funding enabled and organized by Projekt DEAL.

Competing interests

The authors declare no competing interests.

Additional information

Supplementary information The online version contains supplementary material available at <https://doi.org/10.1038/s42003-023-04872-5>.

Correspondence and requests for materials should be addressed to Pawel Brzezowski.

Peer review information *Communications Biology* thanks Krishna Niyogi and the other, anonymous, reviewer for their contribution to the peer review of this work. Primary Handling Editors: Joao Valente.

Reprints and permission information is available at <http://www.nature.com/reprints>

Publisher’s note Springer Nature remains neutral with regard to jurisdictional claims in published maps and institutional affiliations.



Open Access This article is licensed under a Creative Commons Attribution 4.0 International License, which permits use, sharing, adaptation, distribution and reproduction in any medium or format, as long as you give appropriate credit to the original author(s) and the source, provide a link to the Creative Commons license, and indicate if changes were made. The images or other third party material in this article are included in the article's Creative Commons license, unless indicated otherwise in a credit line to the material. If material is not included in the article's Creative Commons license and your intended use is not permitted by statutory regulation or exceeds the permitted use, you will need to obtain permission directly from the copyright holder. To view a copy of this license, visit <http://creativecommons.org/licenses/by/4.0/>.

© The Author(s) 2023